Mon. Not. R. Astron. Soc. **355,** 728–746 (2004) doi:10.1111/j.1365-2966.2004.08352.x

Massive star populations in Wolf–Rayet galaxies

I. F. Fernandes,[1⋆] R. de Carvalho,[2⋆] T. Contini[3⋆] and R. R. Gal[4⋆]

[1]*Instituto Astronômico e Geofísico - USP, Rua do Matão 1226, CEP 05508-900, São Paulo, Brazil*
[2]*INPE/DAS, Av. dos Astronautas, 1.758, CEP 12227-010, São José dos Campos, Brazil*
[3]*Laboratoire d'Astrophysique (UMR 5572), Observatoire Midi-Pyrénées, 14 Avenue Edouard Belin, F-31400 Toulouse, France*
[4]*Department of Physics, UC Davis, One Shields Ave, Davis, CA 95616, USA*

Accepted 2004 August 23. Received 2004 August 4; in original form 2004 May 27

ABSTRACT

We analyse long-slit spectral observations of 14 Wolf–Rayet (WR) galaxies from the sample of Schaerer, Contini & Pindao. All 14 galaxies show broad WR emission in the blue region of the spectrum, consisting of a blend of N IIIλ4640, C IIIλ4650, C IVλ4658 and He IIλ4686 emission lines, which is a spectral characteristic of WN stars. Broad C IVλ5808 emission, termed the red bump, is detected in nine galaxies and C IIIλ5996 is detected in six galaxies. These emission features are due to WC stars. We derive the numbers of late WN and early WC stars from the luminosity of the blue and red bumps, respectively. The number of O stars is estimated from the luminosity of the Hβ emission line, after subtracting the contribution of WR stars. The Schaerer & Vacca models predict that the number of WR stars relative to O stars, $N_{\rm WR}/N_{\rm O}$, increases with metallicity. For low-metallicity galaxies, the results agree with predictions of evolutionary synthesis models for galaxies with a burst of star formation, and indicate an initial mass function (IMF) slope $-2 \lesssim \Gamma \lesssim -2.35$ in the low-metallicity regime. For high-metallicity galaxies our observations suggest a Salpeter IMF ($\Gamma = -2.35$) and an extended short burst. The main possible sources of error are the adopted luminosities for single WCE and WNL stars. We also report, for the first time, on NGC 450 as a galaxy with WR characteristics. For NGC 450, we estimate the number of WN and WC stars. The number ratio $N_{\rm WR}/N_{\rm O}$, and the equivalent widths of the blue bump, EW$_{\lambda4686}$, and of the red bump, EW$_{\lambda5808}$, in NGC 450 are also in good agreement with the instantaneous burst model prediction for WR galaxies.

Key words: galaxies: abundances – galaxies: evolution – galaxies: starburst.

1 INTRODUCTION

Wolf–Rayet (WR) galaxies are extragalactic objects whose spectra show direct signatures similar to those observed in WR stars. The most common characteristic is the presence of a broad He IIλ4686 feature (the blue bump) originating in the stellar winds of WR stars (Schaerer, Contini & Pindao 1999a, hereafter SCP99). WR galaxies have long been known, with the first discovery of such spectral features in the blue compact galaxy He 2–10 (Allen, Wright & Goss 1976). The concept of WR galaxies was introduced by Osterbrock & Cohen (1982, hereafter OC82) and Conti (1991).

The blue WR bump is often blended with nearby nebular emission lines of He, Fe or Ar, and can show several broad stellar emission components (N IIIλ4640, C IIIλ4650, He IIλ4686) which are difficult to deblend in most low- or medium-resolution spectra. These features originate in WR stars of WN and/or WC subtypes (OC82; Conti 1991). The strongest emission line in WC stars is C IVλ5808, which is very weak in WN stars. This 'red WR bump' has only rarely been observed. Where the data are available, C IVλ5808 is generally weaker than He IIλ4686.

In more distant galaxies, WR stars can only be indirectly detected, by observing the integrated spectra of the galaxies. Strong star formation activity indicates the presence of a large number of massive stars, most of which evolve through the WR phase. At a given stage of the starburst, many WR stars appear, but only for a brief duration. Thus, the presence of WR features in these galaxies indicates recent star formation ($<$10 Myr) as well as the presence of massive stars ($M_{\rm initial} > 25$ M$_\odot$; Schaerer, Contini & Kunth 1999b). This provides interesting constraints on recent star formation episodes in these objects (Maeder & Conti 1994). Furthermore, metallicity plays an important role in regulating the lower mass limit above which a star passes through the WR phase.

Despite their small number compared to other massive stars, especially in low-metallicity galaxies, WR stars are numerous enough

⋆E-mail: iran@astro.iag.usp.br (IFF); reinaldo@das.inpe.br (RdC); contini@ast-omp.fr (TC); gal@physics.ucdavis.edu (RRG)

© 2004 RAS

for their integrated emission to be detected. In this paper, we shall follow OC82 and Conti (1991): a WR galaxy is classified as such if its integrated spectrum shows detectable WR broad features emitted by unresolved stellar clusters.

The compilation of Conti (1991) included only 37 objects. Since then, the number of cataloged WR galaxies has increased rapidly, with more than 130 known today (SCP99; Guseva, Izotov & Thuan 2000, hereafter GIT00). WR galaxies do not form a homogeneous class, exhibiting a variety of morphologies. Among the WR galaxies we find low-mass blue compact dwarfs (BCDs), irregular galaxies, massive spirals and ultraluminous merging IRAS galaxies. Recent studies show that WR features are also seen in low-ionization nuclear emission-line regions (LINERs) and Seyfert 2 galaxies (OC82; Ho, Filippenko & Sargent 1995; Heckman et al. 1997; Schmitt, Storchi-Bergmann & Cid Fernandes 1998; Contini et al. 2001). The possibility of detecting WR stars in central cluster galaxies out to a redshift of $z \geqslant 0.25$ is discussed in Allen (1995).

The number of WR stars relative to massive stars is highly dependent on metallicity. Theoretical evolutionary models predict that at fixed metallicity, the ratio between WR and other massive stars varies strongly with the age of the starburst (Maeder 1991; Mas-Hesse & Kunth 1991; Maeder & Meynet 1994; Meynet 1995; Schaerer & Vacca 1998, hereafter SV98). The maximum value of this ratio decreases from 1 to 0.02 when the metallicity decreases from $Z_\odot$ to $Z_\odot/50$ (GIT00). Similarly, the duration of the WR stage in the starburst also decreases with decreasing metallicity. Hence, the number of galaxies with extremely low metallicity containing WR stellar populations is expected to be small.

GIT00 derived the number of WCE and WNL stars from the luminosity of the red and blue bumps, respectively, and the number of O stars from the Hβ luminosity, for 39 WR galaxies with heavy element mass fractions between 1/50 and twice solar. In their sample, the blue bump consists of an unresolved blend of WR and nebular lines. They proposed a new technique to derive the number of WNL stars using N IIIλ4512 and Si IIIλ4565 emission lines. They found that the relative number of WR stars $N_{\rm WR}/N_{\rm (O+WR)}$ and $N_{\rm WC}/N_{\rm WN}$ derived from observations are in satisfactory agreement with theoretical predictions (SV98). The results obtained for the extremely metal-poor galaxies disagree with model predictions likely due to the low emission-line luminosity for WCE stars in metal-poor models.

Using five metal-rich objects from GIT00 and new results on Mrk 309, Schaerer et al. (2000, hereafter SGIT00) attempted to constrain the properties of massive star populations and star formation histories by comparing their observations with evolutionary synthesis models. They found that extended burst durations of ∼4–10 Myr or a superposition of several bursts were required to produce the observed WR population and red supergiant features. The burst durations are longer than those obtained for other objects in Schaerer et al. (1999b) using the same models.

Pindao et al. (2002) analysed the spectra of 85 high-metallicity disc H II regions of nearby spiral galaxies. In contrast with previous studies of low-metallicity galaxies, they found smaller values of I(WR)/I(Hβ) than predicted from evolutionary models at corresponding metallicities. They suggested the use of two WR luminosity regimes to correct the model predictions.

The goal of our study of these 14 galaxies is to search for and confirm the presence of WN and WC stars in galaxies with different metallicities, and to compare the results obtained for this sample with predictions from evolutionary synthesis models (SV98) and Starbust99 (Leitherer et al. 1999). We also report on NGC 450 as a newly classified WR galaxy.

The paper is structured as follows. The observations and procedures used to reduce the data are described in Section 2. In this section we also discuss corrections for reddening and underlying absorption affecting the emission lines. In Section 3 we describe how contamination of a starburst spectrum by the presence of Type IIe supernovae (SN IIe) and active galactic nuclei (AGN) is accounted for, while in Section 4 we explain how the physical parameters of the gas are calculated. The massive star population and constraints on the evolutionary tracks of the starburst regions (age, burst duration and IMF) are derived in Section 5 from a comparison with evolutionary synthesis models. Finally, our main results are summarized and discussed in Section 6.

2 SPECTROSCOPIC OBSERVATIONS AND DATA REDUCTION

2.1 Observations

We observed 14 galaxies from the sample of WR galaxies and extragalactic H II regions presented in SCP99. NGC 6764 was observed at two position angles (PAs), 67° and 90°, with the former along the major axis of the galaxy and the latter spanning a secondary emission region near the central region. We suspected that WR stars may be present in this region, but the spectra do not confirm this hypothesis.

Data were gathered at two different sites. We used the Palomar 200-inch telescope with the long-slit double spectrograph (Oke & Gunn 1982) on 1999 October 10–11 UT, with the 1200 l mm^{-1} grating, blazed at 5000 Å, yielding a pixel size of 0.62 arcsec ×1.3 Å in the blue and 0.47 arcsec ×1.7 Å in the red, and a total wavelength coverage of 3600–6700 Å. The slit width was set to 1 arcsec, resulting in a spectral resolution of ∼5.6 Å in the blue and ∼5.7 Å in the red. The slit length was 180 arcsec. Additional data were taken at the 3.6-m European Southern Observatory (ESO) New Technology Telescope (NTT) telescope using the ESO Multimode Instrument (EMMI) with CCD36 on 1999 April 17 UT. The total wavelength coverage was 4000–6600 Å. The slit width was set to 1 arcsec, resulting in a spectral resolution of ∼5.9 Å. The length of the slit was 120 arcsec.

The slit was aligned along the major axis of the galaxy when possible, and centred on the brightest region of the target. The journal of observations of all objects in the sample is provided in Table 1. Figs 1(a)–(o) show the images of each galaxy taken from the Digitized Sky Survey (DSS) with the slit position overlaid.

2.2 Data reduction

Initial data reduction was carried out following standard procedures with the IRAF[1] task CCDPROC. The package includes bias subtraction, flat-field correction, subtraction of the night sky background and bad column removal. The bias level was subtracted from each frame using the overscan region of the CCD chip.

Spectrum extraction was performed using the IRAF task LONGSLIT. The task includes correction for atmospheric extinction, wavelength calibration and flux calibration. Cosmic rays were removed using the COSMICRAYS task with a threshold of 5 per cent.

[1] IRAF is distributed by the National Optical Astronomy Observatories (NOAO), which are operated by the Association of Universities for Research in Astronomy (AURA) under cooperative agreement with the National Science Foundation.

Table 1. Journal of observations. (α) and (δ) coordinates (J2000) are for the slit centre. The distance (D) is obtained from the redshift measured directly from the object spectrum using $H_0 = 75$ km s^{-1} Mpc^{-1}. NTT and Palomar indicate the observatory where the object was observed. The object type is obtained from the NASA/IPAC Extragalactic Database (NED). The linear scale is obtained using the computed distance, D. For more details on the quoted magnitudes, we refer the reader to the NED.

Galaxy	α (^{h}:^{m}:^{s})	δ ($^\circ$: $'$: $''$)	Exp. time (s)	S/N (Å^{-1})	PA ($^\circ$)	Observation	Type	D (Mpc)	Scale (pc/arcsec)	Mag (Band)
UM 48	0:36:10	4:38:06	3× 1200	96/73	43	Palomar	S	65.22	316	13.35(J)
NGC 450	1:15:31	−0:51:38	1500 + 1200	90/77	80	Palomar	SAB(s)cd	22.46	109	11.40(J)
MRK 712	9:56:42	15:38:04	4× 900	84	108	NTT	SBbc	55.87	271	14.47(B)
MRK 1271	10:56:08	6:10:15	4× 900	80	98	NTT	Compact	8.79	43	14.80(mP)
NGC 4385	12:25:42	0:34:23	4× 900	96	192	NTT	SB(rs)0+	23.35	113	10.64(J)
NGC 4861	12:59:00	34:50:43	1800 + 600	160/97	19	Palomar	SB(s)m	10.93	53	12.44(J)
NGC 5430	14:00:46	59:19:35	2× 1200	140/104	146	Palomar	SB(s)b	40.55	197	10.01(J)
NGC 5471	14:04:29	54:23:49	2× 1200	91/75	127	Palomar	H II	3.86	19	14.76(J)
MRK 475	14:39:05	23:37:28	2× 1800	84/70	80	Palomar	BCD	7.96	39	15.46(B)
Fairall 44	18:13:38	−57:43:59	2× 900	90	105	NTT	S? pec	63.62	308	12.34(J)
NGC 6764	19:08:15	50:55:57	2× 1200	125/95	67/90	Palomar	SB(s)bc	31.26	152	10.56(J)
MRK 309	22:52:34	24:43:50	2× 1500 + 1800	123/90	140	Palomar	Sa	167.09	810	13.05(J)
III Zw 107	23:30:09	25:32:02	1800 + 1200	125/95	175	Palomar	Sb	76.50	371	14.06(J)
NGC 7714	23:36:13	2:09:21	2× 1200	99/71	122	Palomar	SB(s)b:pec	37.05	180	10.77(J)

Spectrophotometric standard stars were observed each night to perform flux calibration. Arc lamps were taken before and after each exposure in order to provide accurate wavelength calibration. An average rms of 0.1 Å was obtained for the pixel to wavelength fit using a third-order spline.

We use a standard extraction aperture for each object, the width of which is such that the peak intensity of the Hβ line decreases by 80 per cent from the centre, along the spatial direction. This width is set independently for each side of the peak. For objects with more than one emission region, different apertures were set for each knot. With this size we obtain the necessary spectral properties for this study while minimizing possible contamination from the adjacent stellar population.

The signal-to-noise (S/N) ratio was determined assuming Poisson statistics and using the readout noise and gain of the CCD, the number of combined spectra and the sky value. For NTT data, the readout noise is 5.43 e^{-1} with a gain of 2.18 e^{-1} per ADU (analogue-to-digital unit). For the Palomar observations, the readout noise is 8.6 e^{-1} with a gain of 2.13 e^{-1} per ADU in the blue channel and 7.5 and 2.00 e^{-1} per ADU in the red channel. The values of the S/N are given in Table 1 for the NTT, as well as the blue and red parts of the Palomar spectra, where they are averages over a range of 100 Å around 4686 and 5878 Å, respectively.

2.2.1 *Reddening correction and underlying Balmer absorption*

The reddening correction is obtained from the Balmer line ratios, using the extinction law of Cardelli, Clayton & Mathis (1989, hereafter CCM89), and the theoretical Balmer emission-line ratios for case B recombination: $I(\mathrm{H}\alpha)/I(\mathrm{H}\beta) = 2.88$ and $I(\mathrm{H}\gamma)/I(\mathrm{H}\beta) = 0.47$ (Brocklehurst 1971). We obtain the colour excess, $E(B-V)$, using the theoretical ratio of Balmer to $F(\mathrm{H}\alpha)/F(\mathrm{H}\beta)$ measurements, according to

$$E(B\text{–}V) = 2.33 \times \left\{ \mathrm{Log}\left[\frac{F(\mathrm{H}\alpha)}{F(\mathrm{H}\beta)}\right] - \mathrm{Log}(2.88) \right\}. \quad (1)$$

In three cases (Mrk 309, Mrk 1271 and Fairall 44) for which $F(\mathrm{H}\alpha)$ is not available, we use solely the measured $F(\mathrm{H}\gamma)/F(\mathrm{H}\beta)$ ratio to obtain the reddening correction using

$$E(B\text{–}V) = 4.71 \times \left\{ \mathrm{Log}\left[\frac{F(\mathrm{H}\gamma)}{F(\mathrm{H}\beta)}\right] - \mathrm{Log}(0.47) \right\}. \quad (2)$$

The resulting colour excess is used to correct each spectrum with the IRAF task DEREDDEN. $E(B-V)$ is easily converted to $cH\beta$ using the relation $E(B-V) \approx 0.677 \times cH\beta$ (Vogel et al. 1993).

In Table 2 we compare the reddening $E(B-V)$ measured in this work with that obtained by other authors. Furthermore, we have compared our derived colour excesses with other measurements taken from the literature in Fig. 2. The top panel shows this comparison, while the bottom panel shows the deviations as a function of $E(B-V)$. The median difference is 0.06 with a standard deviation of 0.18.

We note some differences between the values obtained for some of the objects. The spectroscopic results taken from the literature are inhomogeneous in their instrumental accuracy, observational techniques and the S/N ratios of individual observations. However, it is unlikely that instrumental differences dominate over variations in measured lines intensities due to observing emission from different locations within each galaxy or star formation region, different sized apertures or slightly different PAs used by the authors.

After correcting the spectra for the total interstellar extinction using the Balmer line ratios, some objects show $F(\mathrm{H}\gamma)/F(\mathrm{H}\beta)$ ratios lower than the theoretically predicted values. This effect is more significant for objects where the Hβ equivalent width is less than 70 Å (McCall, Rybski & Shields 1985, hereafter MRS85). The consequence of such underlying absorption is an overestimate of the reddening correction, which is then reflected in all the observed emission lines. To correct for this effect, we use the method proposed by MRS85 to compute the equivalent width in absorption, $\mathrm{EW_{abs}}$, given by the expression

$$\left[\frac{F(\mathrm{H}\gamma)}{F(\mathrm{H}\beta)}\right]_{\mathrm{dered}} = \frac{I(\mathrm{H}\gamma)}{I(\mathrm{H}\beta)} \frac{[1 + \mathrm{EW_{abs}}/\mathrm{EW}(\mathrm{H}\beta)]^{1-\varepsilon}}{[1 + \mathrm{EW_{abs}}/\mathrm{EW}(\mathrm{H}\gamma)]}. \quad (3)$$

The parameter ε is defined by

$$\varepsilon = \frac{[A(\mathrm{H}\gamma)/A_V - A(\mathrm{H}\beta)/A_V]}{[A(\mathrm{H}\alpha)/A_V - A(\mathrm{H}\beta)/A_V]} \quad (4)$$

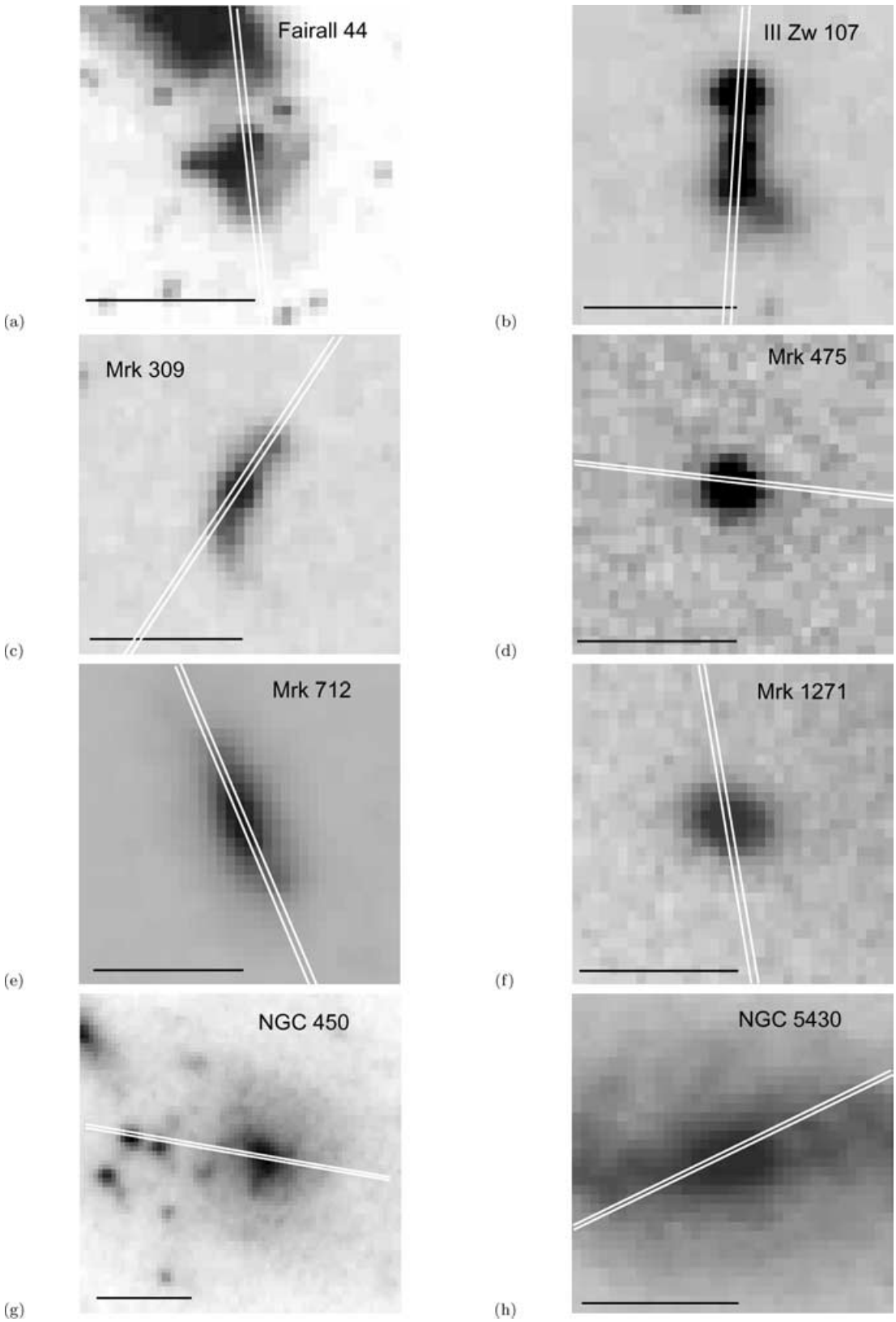

Figure 1. DSS images of galaxies with slit positions: (a) Fairall 44; (b) III Zw 107; (c) Mrk 309; (d) Mrk 475; (e) Mrk 712; (f) Mrk 1271; (g) NGC 450; (h) NGC 4385; (i) NGC 4861; (j) NGC 5430; (k) NGC 5471; (l) NGC 6764 (PA 67°); (m) NGC 6764 (PA 90°); (n) NGC 7714; (o) UM 48. The horizontal bar at the lower left indicates 0.5 arcmin.

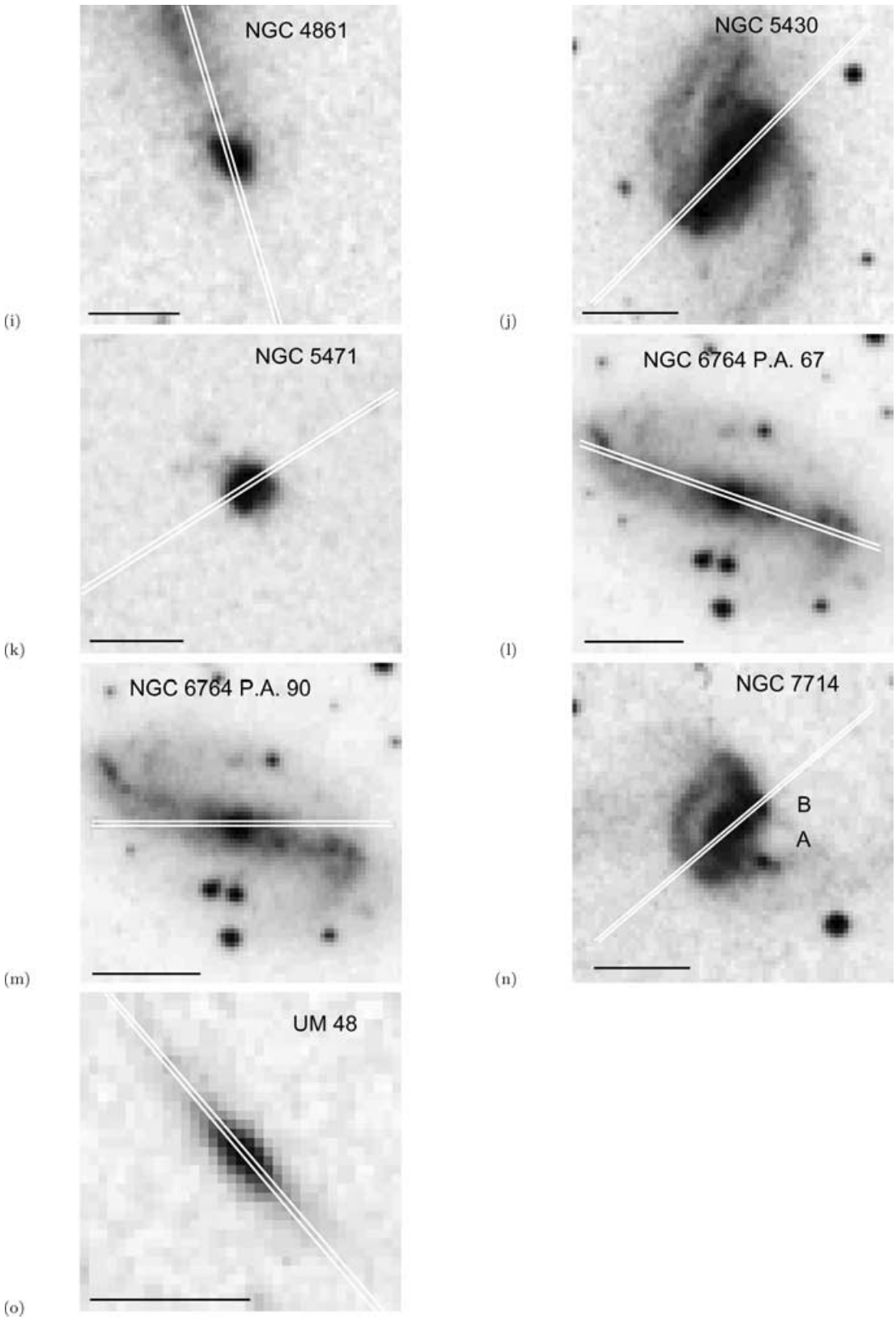

Figure 1 – *continued*

Table 2. $E(B-V)$: comparison with literature. The references cited are as follows: 1, Barth et al. (1994); 2, Calzetti (1997); 3, Contini, Davoust & Considere (1995); 4, Contini et al. (1997); 5, Durret (1990); 6, Eckart et al. (1996); 7, Izotov, Thuan & Lipovetsky (1994); 8, Izotov & Thuan (1998); 9, Gil de Paz et al. (2000); 10, Kell (1982); 11, Mattila & Meikle (2001); 12, Osterbrock & Cohen (1982); 13, Rosa & Benvenuti (1994); 14, Salzer, MacAlpine & Boroson (1989); 15, Vogel et al. (1993).

	Observed	Literature	Reference
Fairall 44	0.47	0.60	5
III Zw 107	0.53	0.47	9
Mrk 309	0.73	0.71, 0.63, 0.70	9, 2, 12
Mrk 475	0.21	0.10	7
Mrk 712	0.03	0.18	3
Mrk 1271	0.15	0.10	8
NGC 450	0.55	–	–
NGC 4385	0.64	0.60, 0.52	2, 14
NGC 4861	0.43	0.20, (0.49, 0.62, 0.77)	2,(1)
NGC 5430	0.67	1.14	4
NGC 5471	0.21	0.15	13
NGC 6764	0.82,0.80	0.61,(0.87)	10, (6)
NGC 7714	0.40	(0.39,041), 0.43	(2), 11
UM 48	0.57	0.49	15

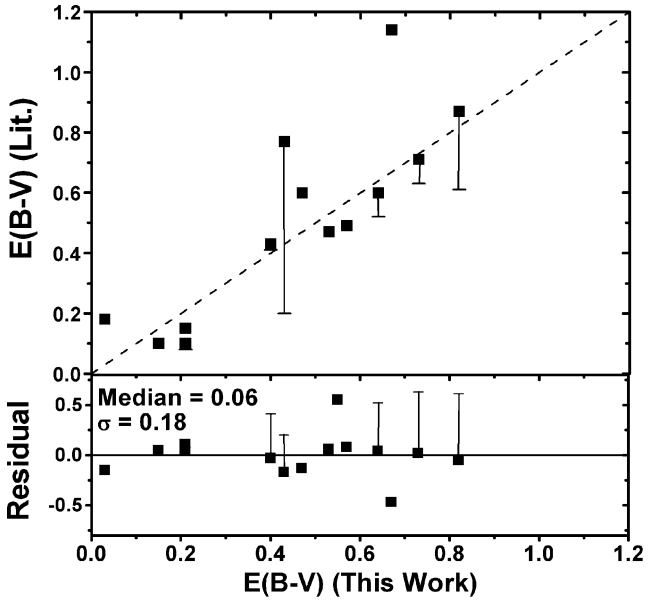

Figure 2. Top: comparison of the values of $E(B-V)$ adopted in this work and those obtained by other authors. The dashed line shows a relation of unity. Bottom: the difference between the values adopted in this work and those obtained by other authors.

and represents the extinction reddening law (MRS85; CCM89).

In the limit $\mathrm{EW_{abs}} = 0$, $[F(\mathrm{H}\gamma)/F(\mathrm{H}\beta)]_{\mathrm{dered}}$ reaches the theoretical ratio $[I(\mathrm{H}\gamma)/I(\mathrm{H}\beta) = 0.47]$. In the opposite limit, as $\mathrm{EW_{abs}}$ approaches unity, the ratio $[F(\mathrm{H}\gamma)/F(\mathrm{H}\beta)]_{\mathrm{dered}}$ is significantly altered from the theoretical expectation. The corrected equivalent widths of the Balmer lines are obtained by adding $\mathrm{EW_{abs}}$ to the observed equivalent widths.

The correction in the extinction due to underlying absorption lines, $E(B-V)_{\mathrm{abs}}$, is given by the expression

$$E(B-V) = -2.33 \times \mathrm{Log}\left\{\frac{1+[\mathrm{EW_{abs}}/\mathrm{EW}(\mathrm{H}\alpha)]}{1+[\mathrm{EW_{abs}}/\mathrm{EW}(\mathrm{H}\beta)]}\right\}. \quad (5)$$

The value of $\mathrm{EW_{abs}}$ for each object is listed in Table 3, along with the equivalent widths of the emission lines EW(Hα), EW(Hβ) and EW(Hγ). Reddening and underlying absorption corrected intensities are also given in the same table.

3 HARD IONIZATION SOURCES

The contamination of a starburst by nearby objects such as SN IIe remnants and AGN could occur, producing WR-like features in the spectrum (Masegosa, Moles & del Olmo 1991). Embedded or superimposed supernova remnants (SNRs) can strongly affect the emission-line properties in a predominantly photoionized H II region (e.g. Peimbert, Sarmiento & Fierro 1991). It is crucial to distinguish between hot stars and other ionizing photon sources. From an observational point of view, the presence of shocks in an ionized nebula can be detected by the enhancement of low excitation lines, in particular [O I], [S II] and [N II] (Masegosa et al. 1991).

We used Veilleux & Osterbrock (1987) diagnostic diagrams to verify the ionization sources in our galaxy sample. Because [S II]$\lambda\lambda$6717, 6731 are not available in our spectra, we use diagnostic diagrams plotting [O I]λ6300/Hα and [N II]λ6584/Hα line ratios against the [O III]λ5007/Hβ ratios (Figs 3 and 4).

The theoretical starburst limits shown in Figs 3 and 4 can be parametrized as

$$\frac{\log([\mathrm{O\,III}]\lambda5007)}{\mathrm{H}\beta} = \frac{0.61}{\log([\mathrm{N\,II}]\lambda6584/\mathrm{H}\alpha) - 0.47} + 1.19 \quad (6)$$

$$\frac{\log([\mathrm{O\,III}]\lambda5007}{\mathrm{H}\beta} = \frac{0.73}{\log([\mathrm{O\,I}]\lambda6300/\mathrm{H}\alpha) + 0.59} + 1.33 \quad (7)$$

given by Kewley et al. (2001). The error range of their modelling in both planes is ±0.1 dex.

All objects in our sample are located in the starburst and H II region loci in the plane of [O I]λ6300/Hα and [N II]λ6584/Hα versus [O III]λ5007/Hβ (Veilleux & Osterbrock 1987), suggesting that the main sources of ionizing photons are stellar, and not AGN.

4 GAS CHEMICAL ABUNDANCES

The oxygen abundance O/H is a crucial parameter for our study because one of the main purposes of this paper is to study the massive star populations in galaxies with different metallicities. In order to obtain the chemical abundances of the galaxies in our sample, three subclasses have been defined depending on whether or not the [O III]λ4363, [O II]λ3727 and [O III]λ λ4959, 5007 features are present (see Kobulnicky, Kennicutt & Pizagno 1999).

(i) Class 1. [O III]λ4363, [O II]λ3727 and [O III]λ λ4959, 5007 are detected. When [O III]λ4363 is detected, the temperature is obtained from the [O III]$\lambda\lambda$5007, 4959/λ4363 line ratio, while the density is measured from the [S II]λ6731/[S II]λ6717 line ratio (McCall 1984). Because our spectra do not include the [S II]$\lambda\lambda$6717, 6731 lines, we are unable to measure the electron density, and we assume a fiducial value of 150 cm^{-3} for n_{e}.

The accuracy of this empirical method depends strongly on an accurate estimate of the electron temperature of the gas (Steigman, Viegas & Gruenwald 1997). The uncertainty in the electron temperature of the gas is directly related to the measurement of the [O III]λ4363 line intensity. The oxygen abundance can be obtained by the empirical method first proposed by Peimbert & Costero (1969), which requires knowledge of the gas temperature and density.

Table 3. Corrected emission-line intensities relative to Hβ = 1000.

	Fairall 44	III Zw 107	Mrk 309	Mrk 475	Mrk 712	Mrk 1271
[O II]λ3727	–	2213±12	703±98	1093±4	–	–
[Ne III]λ3869	–	259±5	–	362.9±2.7	–	–
Hγ	475±2	470±5	466±46	470±3	470±3	470±8
[O III]λ4363	26±9	13±4	–	85±3	14±2	61±12
He Iλ4471	53±9	49±5	59±38	42±2	67±2	61±15
[Fe III]λ4656	29±5	13±7	131±29	5±3	14±3	26±7
He IIλ4686	19±5	3±9	–	17±4	–	35±11
[Ar IV]λ4711	–	14±10	–	8±3	8±2	–
[Ar IV]λ4740	–	–	–	7±3	–	–
He Iλ4922	–	12±8	–	11±3	19±2	–
[O III]λ4959	710±5	1215±7	104±25	1781±5	1613±4	1115±12
[O III]λ5007	2061±9	3632±18	381±33	5326±15	4881±11	3096±29
[N I]λ5199	–	31±7	–	4±3	12±3	–
[Fe III]λ5271	–	–	–	7±3	10±3	–
[Cl III]λ5518	–	10±2	–	8±2	8±5	–
[Cl III]λ5538	–	3±1	–	4±2	6±5	–
[N II]λ5754	–	9±2	38±25	5±3	7±3	–
He Iλ5876	126±4	129±2	24±17	99±1	228±3	119±9
[O I]λ6300	48±6	53±2	26±22	24±1	36±3	65±11
[S III]λ6313	8±4	11±2	–	24±1	24±3	15±10
[O I]λ6364	18±4	18±3	–	9±1	12±3	72±11
[N II]λ6548	–	98±2	–	33±2	268±2	84±11
Hα	–	2855±14	–	2870±8	–	2899±25
[N II]λ6584	–	280±2	–	66±1	–	221±9
EW(Hγ) (Å)	32.17±0.23	26.65±0.35	3.00±0.18	73.08±3.35	45.98±0.21	15.42±0.20
EW(Hβ) (Å)	67.64±0.26	65.48±0.46	10.18±0.79	140.50±0.37	139.10±0.29	33.11±0.28
EW(Hα) (Å)	–	329.60 ±3.70	–	936.20±10.98	–	109.20±1.16
EW_{abs} (Å)	–	–0.98	–	–1.18	–	–0.69
F(Hβ) (10^{-14} erg s^{-1} cm^{-2})	3.58±0.01	12.77±0.06	12.8±1.04	7.52±0.03	2.45±0.02	0.72±0.01
$E(B-V)$	0.47	0.53	0.73	0.21	0.03	0.15
$E(B-V)_{abs}$	–	−0.012	–	−0.007	–	−0.015
Broad emission lines						
N IIIλ4640	–	7±5	167±33	–	82±10	–
He IIλ4886	59±9	61±26	115±20	69±16	98±7	103±41
C IIIλ5696	–	–	15±4	–	–	–
C IVλ5808	–	–	–	36±7	–	–
EWλ4640(Å)	–	0.37±0.38	1.36±0.21	–	7.23±0.98	–
EWλ4686(Å)	3.47±0.56	3.60±2.86	0.97±0.20	9.51±2.35	8.67±0.74	3.06±1.21
EWλ5696(Å)	–	–	0.26±0.05	–	–	–
EWλ5808(Å)	–	–	–	8.02±1.46	–	–

(ii) Class 2. [O III]λ4363 is not detected, while [O II]λ3727 and [O III]λ λ4959, 5007 are detected. For those galaxies where the [O III]λ4363 auroral line is not detected, the oxygen abundance is obtained from the empirical calibration suggested by McGaugh (1991) using the known R_{23} ratio, ([O II]λ3727+[O III]λλ5007, 4959)/ Hβ.

The relation between oxygen abundance and R_{23} is double valued, but this degeneracy can be broken. We use the relation between [N II]λ6584/[O II]λ3727 and [N II]λ6584/Hα ratios to break the O/H versus R_{23} degeneracy (Contini et al. 2002).

Kobulnicky et al. (1999) provide a polynomial fit to both metal-poor (lower branch)

$$12 + \log(\mathrm{O/H})_{\mathrm{l}} = 12 - 4.944 + 0.767x + 0.0602x^2 - y(0.29 + 0.332x - 0.331x^2), \quad (8)$$

and metal-rich (upper branch) regimes

$$12 + \log(\mathrm{O/H})_{\mathrm{u}} = 12 - 2.939 - 0.2x - 0.237x^2 - 0.305x^3 - 0.0283x^4 - y(0.0047 - 0.0221x - 0.102x^2 - 0.0817x^3 - 0.00717x^4), \quad (9)$$

where

$$x \equiv \log R_{23} \equiv \log([\mathrm{O\,II}]\lambda3727 + [\mathrm{O\,III}]\lambda\lambda5007, 4959)/\mathrm{H}\beta) \quad (10)$$

and

$$y \equiv \log O_{32} \equiv \log([\mathrm{O\,III}]\lambda\lambda5007, 4959)/[\mathrm{O\,II}]\lambda3727). \quad (11)$$

The R_{23} calibration has an estimated uncertainty of ±0.10 in log(O/H) (Kobulnicky et al. 1999).

(iii) Class 3. [O II]λ3727 is not detected, but [O III]λ4363 and [O III]λ λ4959, 5007 are detected (NTT data). It is not possible to break the degeneracy using the [N II]λ6584/[O II]λ3727 and [N II]λ6584/Hα ratios.

In this case, we can derive the electron temperature but not the O/H abundance. We use the temperature obtained from standard nebular analysis to select the appropriate metallicity calibration with which we derive the oxygen abundance. After determining the metallicity regime for each galaxy, we compute the O/H ratio using the upper

Table 3 – *continued*

	NGC 450	NGC 4385	NGC 4861	NGC 5430	NGC 5471	NGC 6764
[O II]λ3727	1615±3	–	626±2	1491±28	919±2	1933±29
[Ne III]λ3869	240±2	–	408±2	–	399±2	68±18
Hγ	481±2	471±3	470±2	470±23	470±2	470±12
[O III]λ4363	27±2	13±3	89±2	–	66±2	21±8
He Iλ4471	48±2	30±6	37±2	46±9	39±2	47±13
[Fe III]λ4656	9±3	35±6	8±3	49±23	26±4	69±22
He IIλ4686	–	14±4	8±2	32±10	25±1	54±15
[Ar IV]λ4711	5±2	–	11±2	–	14±1	–
[Ar IV]λ4740	–	–	7±2	–	–	–
He Iλ4922	13±2	–	5±2	–	9±1	–
[O III]λ4959	1368±3	231±3	1817±4	129±10	1850±30	168±6
[O III]λ5007	3864±7	678±4	5521±11	375±12	5583±90	484±8
[N I]λ5199	9±2	19±3	3±3	12±12	–	88±14
[Fe III]λ5271	6±3	–	–	–	2±2	–
[Cl III]λ5518	6±1	–	4±2	1±1	5±1	7±5
[Cl III]λ5538	5±1	–	3±2	2±2	6±2	–
[N II]λ5754	2±1	10±3	–	12±4	3±2	29±7
He Iλ5876	131±1	127±3	92±1	119±5	111±1	123±6
[O I]λ6300	25±1	25±4	16±2	–	22±1	159±7
[S III]λ6313	15±1	10±4	17±2	6.7±3.3	18.6±0.7	–
[O I]λ6364	9±1	6±5	5±1	4±3	8±1	67±8
[N II]λ6548	71±1	503±4	23±2	441±11	46±1	726±12
Hα	2872±5	2884±8	2855±22	2837±49	2866±5	2806±35
[N II]λ6584	167±1	1489±5	47±2	1207±22	93±1	1914±24
EW(Hγ) (Å)	93.61±0.31	13.85±0.09	48.25±0.32	13.21±0.45	51.68±0.18	6.58±0.14
EW(Hβ) (Å)	320.80±0.59	42.78±0.11	156.80±0.29	40.85±0.41	181.20±0.29	22.46±0.27
EW(Hα) (Å)	2928.00±10.59	199.10±1.66	938.00±5.61	264.60±1.25	1028.00±6.35	136.40±0.90
EW_{abs} (Å)	−0.27	−2.18	0.00	−0.05	−0.40	−0.72
F(Hβ) (10^{-14} erg s^{-1} cm^{-2})	30.78±0.06	48.63±0.15	103.60±0.20	37.17±0.63	7.73±0.01	59.81±0.83
$E(B-V)$	0.55	0.64	0.43	0.67	0.21	0.82
$E(B-V)_{abs}$	−0.001	−0.039	0.000	−0.001	−0.002	−0.027
Broad emission lines						
N IIIλ4640	21±16	95±11	–	127±26	–	161±33
He IIλ4886	31±14	103±8	55±13	105±18	22±4	63±21
C IIIλ5696	–	31±31	3±2	–	–	10±5
C IVλ5808	23±3	62±34	11±6	41±10	–	74±27
EWλ4640(Å)	5.14±3.80	3.53±0.39	–	5.50±0.94	–	2.94±0.61
EWλ4686(Å)	7.61±3.80	3.91±0.26	7.08±1.75	3.61±0.78	3.14±0.69	1.15±0.57
EWλ5696(Å)	–	2.16±2.12	0.81±0.47	–	–	0.30±0.18
EWλ5808(Å)	10.58±1.60	4.55±2.41	3.00±1.49	3.16±1.77	–	3.90±0.76

branch given by Edmunds & Pagel (1984),

$$\log(\mathrm{O/H})_{\mathrm{u}} \simeq -0.69 \log R_3 - 3.24, \quad (12)$$

$$(0.6 \leqslant \log R_3 \leqslant 1.0)$$

$$R_3 \equiv \frac{F_{[\mathrm{O\,III}]}\lambda\lambda 5007, 4959}{F_{\mathrm{H}\beta}}$$

for galaxies in the high-metallicity regime, and the lower branch

$$\log(\mathrm{O/H})_{\mathrm{l}} \simeq 1.67 \log R_3 + 6.43, \quad (13)$$

$$(0.4 \leqslant \log R_3 \leqslant 1.1)$$

for low-metallicity objects. The R_3 calibration has an estimated uncertainty of ±0.20 in log(O/H) (Edmunds & Pagel 1984).

Two additional empirical tools were used to obtain the oxygen abundance: the P–R_{23} calibration, with an estimated uncertainty of 0.10 dex (Pilyugin 2000, 2001a,b), and the [O III]/[N II] calibration given by Pettini & Pagel (2004), with an uncertainty of 0.25 dex. In particular, for NTT data we use the calibration extrapolated to [O II]λ3727 = 0, where the uncertainty increases to 0.30 dex (Pilyugin 2001a).

To compare the derived oxygen abundances, we use as many of the methods described above as possible (based on available spectral features) to derive O/H values for all of the galaxies in our sample. Fig. 5 shows the comparison between results obtained applying the T_{e} method and the other methods used in this work. We see that, in the absence of [O III]λ4363, use of the electron temperature T_{e}, the R_{23} method (for Class 2 objects) and the [O III]/[N II] calibration all provide good determinations of gas abundance. The R_3 technique was used only for MRK 712. We find that the R_{23} and R_3 calibrations of Pilyugin do not perform correctly for either high or very low gas abundances, and are therefore not used in this work.

Furthermore, in Fig. 6 we have compared our derived gas abundances with those in the literature. The top panel shows this comparison, while the bottom panel shows the deviations as a function

Table 3 – *continued*

	NGC 6764 (PA 90°)	NGC 7714A	NGC 7714B	UM 48
[O II]λ3727	1703±31	1970±8	2107±10	2152±29
[Ne III]λ3869	130±23	95±3	280±4	111±15
Hγ	471±15	472.4±3.7	469.9±4.4	472±16
[O III]λ4363	19±8	13.6±4.2	39.3±4	12±6
He Iλ4471	59.7±16.5	39.6±3.5	46±4	54±18
[Fe III]λ4656	85±26	30±5	28±9	35±23
He IIλ4686	58±23	6±1	4±4	12±16
[Ar IV]λ4711	–	–	22±7	-
[Ar IV]4740	–	–	–	–
He Iλ4922	–	–	12±4	–
[O III]λ4959	171±8	496±40	1180±6	518±14
[O III]λ5007	484±11	1550±140	3529±14	1563±20
[N I]λ5199	77±15	18±4	–	–
[Fe III]λ5271	–	27±4	23±4	–
[Cl III]λ5518	10.7±9	7±4	–	–
[Cl III]λ5538	4.2±6	7±4	–	–
[N II]λ5754	20±7	11±3	11±10	–
He Iλ5876	99±7	125±3	117±3	125±5
[O I]λ6300	156±8	44±4	46±4	34±10
[S III]λ6313	–	8±4	15±4	15±11
[O I]λ6364	58±8	14±6	16±4	13±7
[N II]λ6548	708±13	362±4	131±4	197±5
Hα	2811±40	2823±123	2872.2±12	2869±31
[N II]λ6584	1912±28	923±5	334±4	573±8
EW(Hγ) (Å)	6.39±0.17	12.13±0.08	68.88±0.57	9.95±0.31
EW(Hβ) (Å)	22.04±0.30	32.99±0.10	191.30±0.72	29.25±0.31
EW(Hα) (Å)	137.70±0.97	98.48±0.63	12.00±0.01	156.30±1.09
EW_{abs} (Å)	−0.94	−1.44	−0.18	−1.29
F(Hβ) (10^{-14} erg s^{-1} cm^{-2})	48.98±0.80	86.15±0.32	7.79±0.03	9.32±0.12
$E(B-V)$	0.80	0.52	0.40	0.57
$E(B-V)_{abs}$	−0.036	−0.029	−0.014	−0.035
Broad emission lines				
N IIIλ4640	161±39	41±9	–	–
He IIλ4886	64±23	22±10	54±14	56±33
C IIIλ5696	10.±7	5.0±0.6	–	–
C IVλ5808	81±29	34±14	–	22±12
EWλ4640(Å)	2.94±0.71	1.41±0.25	–	–
EWλ4686(Å)	1.20±0.54	0.60±0.27	10.34±2.92	1.50±0.84
EWλ5696(Å)	0.23±0.17	0.22±0.03	–	–
EWλ5808(Å)	3.65±0.69	1.77±0.08	–	1.52±0.71

of 12 + log(O/H). The median difference is 0.02 dex with a standard deviation of 0.17 dex.

The above comparisons, both internal and external, demonstrate that our gas abundance determinations are reliable and robust. The gas abundances must be measured correctly to accurately constrain the massive stellar population and its relation to gas metallicity. The abundances obtained using the different methods and the final adopted value for the oxygen abundance of each galaxy are listed in Table 4.

5 MASSIVE STAR POPULATIONS: WR AND O STAR NUMBERS

The number of massive stars present in a region of a WR galaxy can be derived using the standard method developed by Conti (1991). A representative number of O and WR subtype stars can be obtained directly from the optical spectra (Vacca & Conti 1992, hereafter VC92).

The absolute number of WR stars in the sampled galaxies was estimated using the blue bump (λ4686) and red bump (λ5808) luminosities. The blue bump is a blend of NVλ4605, N IIIλλ4634, 4640, C IIIλ4650, C IVλ4658 and He IIλ4686 broad WR lines (GIT00). Superposed on the blue bump may be [Fe III]λ4658, He IIλ4686 and [Ar IV]λλ 4711, 4740, which are narrow nebular lines. The dominant contribution to the blue bump is from the broad He IIλ4686 line arising in WNL stars, while the red bump is mainly due to broad C IVλ5808 from WC stars (Schaerer et al. 1999b; GIT00). However, some contribution from early WN stars (WNE) might be present in the blue bump (SV98). The detectability of the red bump is low compared to the blue bump. Fig. 7 shows the spectral region of those galaxies in our sample containing either the blue bump or the red bump.

The dominant subtype of WR stars can be constrained by analysing the presence of particular lines. N IIIλ4640 and/or C IIIλ4650 are observed in nine galaxies, while NVλ4604 is absent. The former are due only to WN stars, thus indicating the predominance of WNL stars (SGIT00).

To derive the number of WNL stars from the blue bump, we measured the flux of the entire bump, and then subtracted the nebular

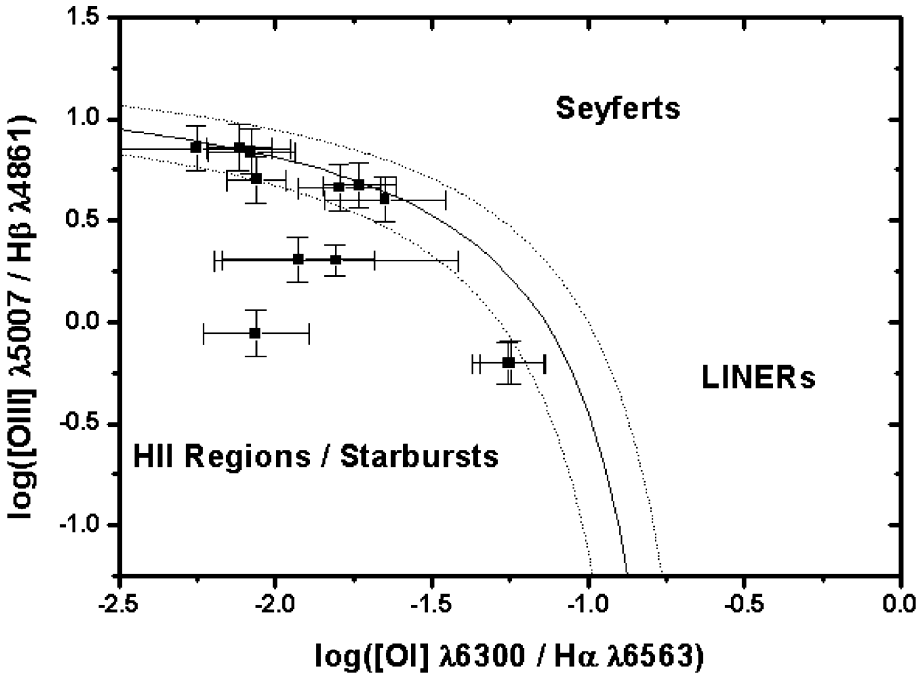

Figure 3. The diagnostic diagram of [O III]λ5007/Hβ plotted against [O I]λ6300/Hα. The solid line shows the border between starburst and AGN ionization mechanisms. The dashed lines show the model uncertainty of 0.1 dex.

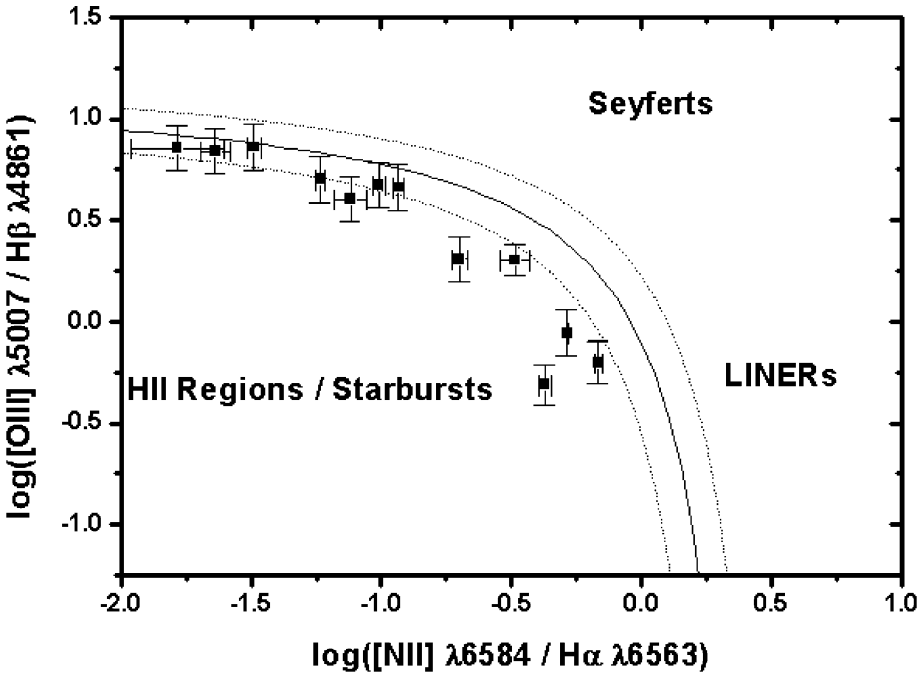

Figure 4. The diagnostic diagram of [O III]λ5007/Hβ plotted against [N II]λ6584/Hα. The solid line shows the border between starburst and AGN ionization mechanisms. The dashed lines show the model uncertainty of 0.1 dex.

lines and the contributions of N IIIλ4640 and C III/C IVλ4650/λ4658 when these lines were present. This procedure then retains only the broad emission component of He IIλ4686.

The C IIIλ5696 emission line is a signature of late-type WC stars (WCL; GIT00), and their presence is expected in high-metallicity regions (Maeder 1991). When C IIIλ5696 is absent, but C IVλ5808 is present, the emission is likely due to early-type WC stars (WCE). WN stars cannot be responsible for the C IVλ5808 emission, because the ratio He IIλ4686/C IVλ5808 observed in our spectra ranges from 0.64 to 5, much lower than the value of $\sim$16 predicted by SV98 (SGIT00).

The absolute population of WR subtype stars can be derived if the line luminosity of a single subtype star is known. We use the integrated broad emission-line luminosity of He IIλ4686 in each of

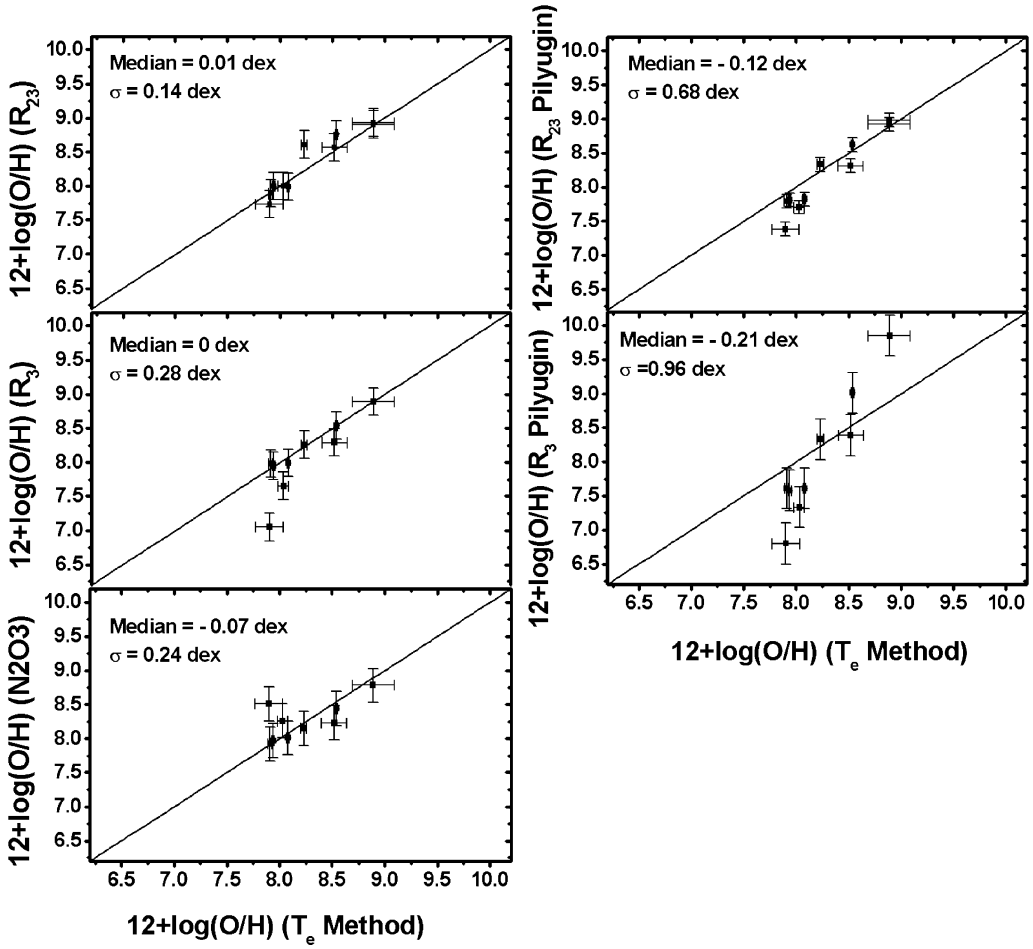

Figure 5. Comparison between the values of 12 + log(O/H) obtained with the T_e method and other methods used in this work. The median offset and σ for each relation are noted in each panel. The R_{23} and R_3 calibrations of Pilyugin are shown separately on the left.

our galaxies to derive the number of WNL stars, the C IVλ5808 luminosity to derive the number of WCE stars, and C IIIλ5696 for WCL stars (GIT00).

In practice,

$$N_{\rm WNL} = \frac{L^{\rm obs}_{\rm He\,II\lambda4686}}{L_{\rm He\,II\lambda4686}}, \tag{14}$$

$$N_{\rm WCE} = \frac{L^{\rm obs}_{\rm C\,IV\lambda5808}}{L_{\rm C\,IV\lambda5808}}, \tag{15}$$

and

$$N_{\rm WCL} = \frac{L^{\rm obs}_{\rm C\,III\lambda5696}}{L_{\rm C\,III\lambda5696}}, \tag{16}$$

where $L^{\rm obs}_{\rm He\,II\lambda4686}$, $L^{\rm obs}_{\rm C\,IV\lambda5808}$ and $L^{\rm obs}_{\rm C\,III\lambda5696}$ are the total luminosities observed around the corresponding spectral features. For the average luminosity of a single WNL star in the He IIλ4686 line we use $L_{\rm He\lambda4686} = 1.6 \pm 0.8 \times 10^{36}$ erg s^{-1}, while for a single WCE star in the C IVλ5808 line we use $L_{\rm C\,IV\lambda5808} = 3.0 \pm 1.1 \times 10^{36}$ erg s^{-1}, and for a single WCL star in the C IIIλ5696 line we use $L_{\rm C\,III\lambda5696} = 8.1 \pm 2.9 \times 10^{35}$ erg s^{-1} (SV98).

Then, the total number of WR stars is defined by

$$N_{\rm WR} = N_{\rm WCE} + N_{\rm WCL} + N_{\rm WNL}. \tag{17}$$

We note that these line luminosities are based on WR stars observed in the Milky Way, assuming solar metallicity. The line luminosities show significant scatter depending on the dominant WR subtype and the metallicity in the observed object.

To obtain the number of O stars in each galaxy, we assume that all ionizing photons, Q_0, are produced by O and WR stars (Conti 1991). Hence,

$$Q^{\rm obs}_0 = N_{\rm O7V} Q_{\rm O7V} + N_{\rm WR} Q_{\rm WR} \tag{18}$$

where $N_{\rm O7V}$ is the number of O7V stars and $Q_{\rm WR}$ and $Q_{\rm O7V}$ are the number of ionizing photons per second produced by WR stars (all subtypes summed up) and O7V stars, respectively. Thus, the total number of ionizing photons can be obtained from the Hβ luminosity, L(Hβ), through the relation

$$Q^{\rm obs}_0 = 2.01 \times 10^{12} L_{\rm H\beta}. \tag{19}$$

The number of O stars present is derived from the number of O7V stars after applying a correction for the presence of other O star subtypes. In this sense, VC92 and Vacca (1994) defined the conversion parameter as the proportion of O7V stars relative to all OV stars:

$$\eta_0 = N_{\rm O7V}/N_{\rm OV}. \tag{20}$$

The parameter η_0 depends on the IMF for massive stars and is a function of the time elapsed since the beginning of the burst.

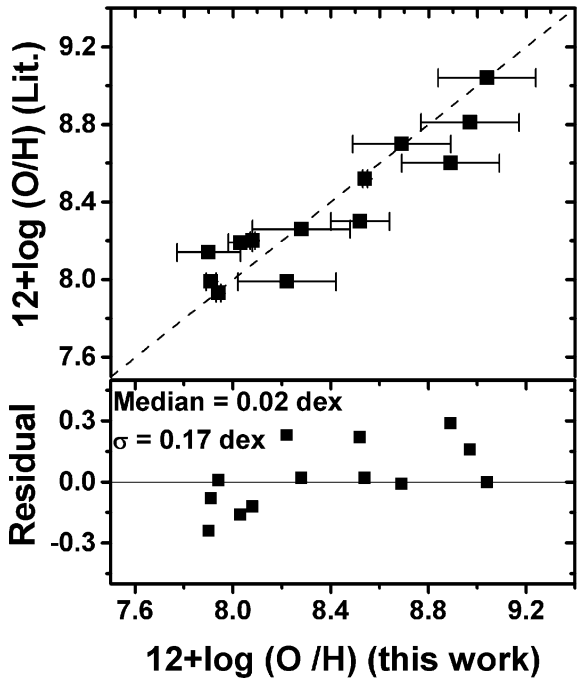

Figure 6. Top: comparison of the values of 12 + log(O/H) adopted in this work and those obtained by other authors. The dashed line shows a relation of unity. Bottom: the difference between the values obtained by other authors and those adopted in this work.

Using the models of SV98, which give the evolution of EW(Hβ) as a function of the time elapsed from the beginning of an instantaneous burst for different metallicities, we derive the starburst age t for each of our galaxies. These ages are in good agreement with the predicted age and duration of the WR phase estimated from instantaneous burst models. We use the models of SV98 to evaluate the parameter $\eta_0(t)$, adopting the oxygen abundance obtained for objects as the metallicity, the canonical slope for a Salpeter IMF $\Gamma = -2.35$, and a stellar mass upper limit of 120 $M_\odot$. The number of ionizing photons, the age of the starburst and $\eta(t)$ derived for each galaxy of our sample are given in Table 5.

Then, using equations (18), (19) and (20), the absolute number of O stars can be derived as

$$N_{\rm O} = N_{\rm OV} = \frac{Q_0^{\rm obs} - N_{\rm WR} Q_{\rm WR}}{\eta_0(t) Q_{\rm O7V}}. \quad (21)$$

We adopt $Q_{\rm WR} = Q_{\rm O7V} = 1.0 \times 10^{49}$ s^{-1} (Schaerer et al. 1999b).

The absolute number of O stars, WR stars, $N_{\rm WNL}$ and $N_{\rm WCE}$, and the ratio $N_{\rm WR}/N_{\rm O}$ are given in Table 6.

5.1 Comparison with evolutionary models

The relationship between the $N_{\rm WR}/N_{\rm O}$ ratio and oxygen abundance obtained for the galaxies in our sample is shown in Fig. 8. We adopt a solar oxygen abundance of 12 + log(O/H) = 8.70 (Grevesse & Anders 1989; Grevesse & Sauval 1998). The predictions of SV98 models for instantaneous bursts (solid line) with IMF slopes of -1, -2 and -2.35 (Salpeter), and of Starburst99 (Leitherer et al. 1999) for extended bursts (duration of 2–4 Myr) with IMF slope = -2.35 and mass limit of 100 $M_\odot$ (dashed line) are plotted.

Evolutionary models predict that, for a given metallicity, the ratio between WR and O stars varies strongly with the age of the burst, and the duration of the WR stage in the starburst also increases with increasing metallicity (Maeder & Meynet 1994; Meynet 1995; SV98). Maeder (1991) interpreted this behaviour as the result of increased stellar mass loss at higher metallicities. The increased stellar mass loss reduces the mass limit for forming WR stars in metal-rich galaxies (Maeder 1991).

In the low-metallicity case, the results can be explained by an instantaneous burst with a Salpeter IMF slope ($\Gamma = -2$ to -2.35). In the high-metallicity regime, the results deviate from the expected behaviour based on models with an instantaneous burst for starburst galaxies (SV98). A steeper IMF slope is required than in the low-metallicity case, or we must invoke an extended burst to explain the results. SGIT00 interpret this behaviour for their sample of high-metallicity galaxies as implying an extended burst duration of ∼4–10 Myr. Support for this

Table 4. Oxygen abundance obtained using different methods. The references cited are as follows: (a) Contini et al. (1995); (b) Contini et al. (1997); (c) Evans (1986); (d) Gil de Paz et al. (2000); (e) GIT2000; (f) González-Delgado et al. (1995); (g) Masegosa et al. (1991); (h) SGTI 2000; (i) Sugai & Taniguchi (1992).

Method	R branch	$T_{\rm e}$	R_{23}	N2O3	R_3	R_{23} Pilyugin	R_3 Pilyugin	Adopted	Δ Max	Literature
Fairall 44	Upper	–	–	–	8.45	–	8.26	8.45±0.20	0.19	–
III Zw 107	Upper	8.52±0.12	8.57	8.23	8.29	8.31	8.39	8.52±0.12	0.34	8.30(d)
Mrk 309	Upper	–	9.04	–	8.98	9.40	10.07	9.04±0.20	1.09	9.03(h)
Mrk 475	Lower	7.94±0.01	8.00	7.97	7.95	7.81	7.58	7.94±0.01	0.39	7.93(e)
Mrk 712	Upper	–	–	–	8.28	–	8.37	8.28±0.20	0.09	8.26(a)
Mrk 1271	Lower	–	–	8.22	7.57	–	8.49	8.22±0.20	0.92	7.99(e)
NGC 450	Upper	8.23±0.03	8.61	8.15	8.26	8.33	8.33	8.23±0.03	0.18	–
NGC 4385	Upper	–	–	8.69	8.79	–	9.61	8.69±0.20	0.92	8.70(i)
NGC 4861	Lower	7.91±0.02	7.89	7.92	7.98	7.79	7.61	7.91±0.02	0.37	7.99(e)
NGC 5430	Upper	–	8.97	8.75	8.97	9.08	10.04	8.97±0.20	1.29	8.81(b)
NGC 5471	Lower	8.08±0.01	7.99	8.01	7.99	7.82	7.61	8.08±0.01	0.38	8.20(c)
NGC 6764	Upper	8.89±0.20	8.90	8.78	8.89	8.92	9.85	8.89±0.20	1.07	8.60(b)
NGC 6764	Upper	8.89±0.20	8.93	8.78	8.89	8.98	9.85	8.89±0.20	1.07	–
NGC 7714A	Lower	7.90±0.13	7.73	8.51	7.05	7.38	6.80	7.90±0.13	1.71	8.14(f)
NGC 7714B	Lower	8.03±0.05	8.00	8.26	7.65	7.70	7.33	8.03±0.05	0.93	8.19(f)
UM 48	Upper	8.54±0.01	8.76	8.44	8.54	8.62	9.01	8.54±0.01	0.57	8.52(g)

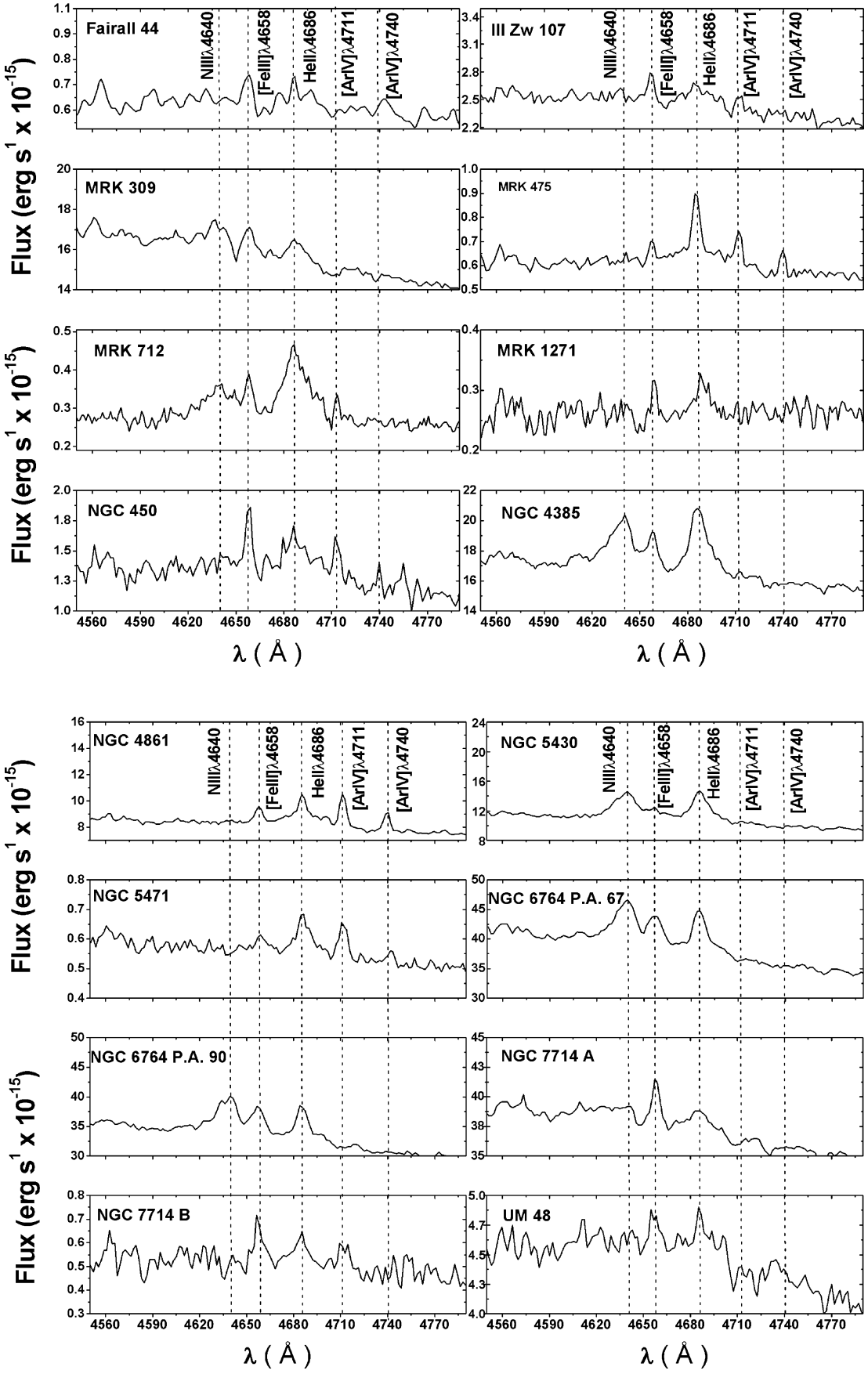

Figure 7. Enlargement of blue and red bump spectral regions of galaxies where the broad lines He IIλ4686 and C IVλ5808 are visible.

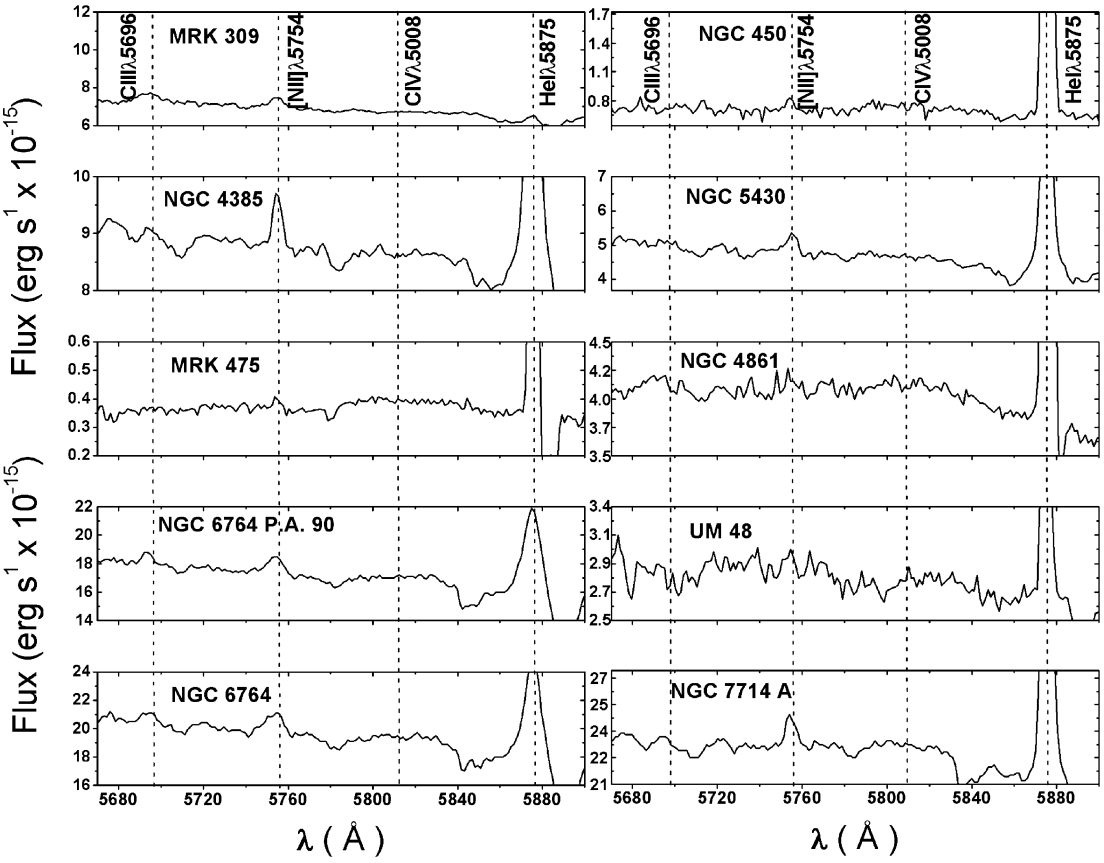

Figure 7 – *continued*

Table 5. Star population parameters.

	Q_0 ($\times 10^{52}$)	Age (Myr)	$\eta_0(t)$
Fairall 44	3.96±0.59	3.0	0.50
III Zw 107	18.61±2.79	4.0	0.53
Mrk 309	89.76±13.46	6.1	0.80
Mrk 475	0.12±0.02	4.1	0.48
Mrk 712	2.27±0.34	3.5	0.86
Mrk 1271	0.04±0.01	4.7	0.36
NGC 450	3.52±0.53	2.6	1.50
NGC 4385	9.85±1.48	4.9	0.18
NGC 4861	3.18±0.48	4.0	0.53
NGC 5430	15.28±2.29	5.1	0.14
NGC 5471	0.03±0.00	3.8	0.65
NGC 6764	14.94±2.24	5.5	0.12
NGC 6764	12.40±1.86	5.5	0.12
NGC 7714A	29.68±4.45	5.4	0.52
NGC 7714B	2.79±0.42	3.7	0.72
UM 48	9.94±1.49	4.8	0.20

conclusion comes from the observed WR population relation (WC/WN) with metallicity and the red supergiant star features observed in their objects (GIT00; SGIT00). NGC 4385, 5430, 6764 and UM 48, with $12 + \log(\mathrm{O/H}) > 8.4$, are candidates for this type of object.

In Fig. 9 we plot the ratio $N_{\mathrm{WC}}/N_{\mathrm{WN}}$ (where WC = WCL + WCE) versus oxygen abundance compared to the predictions of SV98 models for an instantaneous burst, as well as extended bursts of 2 and 4 Myr (Pindao et al. 2002). The dot-dashed line (bottom right) shows the observed trend of WC/WN with metallicity in Local Group galaxies derived empirically from observations by Massey & Johnson (1998). The $N_{\mathrm{WC}}/N_{\mathrm{WN}}$ ratio is lower than the instantaneous burst model predictions and, for galaxies with metallicity higher than $12 + \log(\mathrm{O/H}) > 8.4$, the ratio is closest to the values reported for galaxies in the Local Group corresponding to a constant star formation regime (Massey & Johnson 1998).

These low $N_{\mathrm{WC}}/N_{\mathrm{WN}}$ ratios might be partially explained by the assumption that the predominant contribution to the C IVλ5808 line luminosity at high metallicities is from WCE stars. If instead we assume that the main contribution to this line luminosity comes from WCL stars, the lower luminosity of WCL stars can increase the ratio of WC to WN stars by a factor of ∼3–4 (GIT00). SV98 predict a luminosity ratio C IIIλ5696/C IVλ5808 for a WCL (WC7) star of ∼0.5, but galaxies in our sample where WC emission lines are measured show lower C IIIλ5696/C IVλ5808 ratios.

We contend that the low $N_{\mathrm{WC}}/N_{\mathrm{WN}}$ ratios observed in high-metallicity galaxies are due to the nature of the star formation bursts, with different durations for the WN and WC stages (GIT00). These galaxies have low Hβ equivalent widths leading to ages greater than 5.3 Myr (except UM 48 with age ≃4.8 Myr). They are therefore in the late stages of their WR episodes (GIT00). At these later times, WN stars are still present, while the number of WC star drops to zero (SV98). This supports an extended burst to explain the $N_{\mathrm{WN}}/N_{\mathrm{O}}$ ratio seen in these galaxies.

The presence of late-type stellar features provides additional evidence supporting an extended burst. These absorption features are commonly observed in integrated spectra of stellar clusters,

Table 6. Massive star population.

	$N_{\rm WNL}$	$N_{\rm WCL}$	$N_{\rm WCE}$	$N_{\rm WR}$	$N_{\rm O}$	$N_{\rm WR}/N_{\rm O}$*	$N_{\rm WC}/N_{\rm WN}$*
Fairall 44	692±363	–	–	692±363	5660±623	0.12±0.04	–
III Zw 107	3389±2211	–	–	3389±2211	28726±4172	0.13±0.04	–
Mrk 309	30841±16314	7945±229	–	38786±16315	58498±16883	0.66±0.24	0.26±0.09
Mrk 475	25±14	–	7±3	32±14	186±29	0.17±0.16	0.28±0.10
Mrk 712	661±334	–	–	661±334	1876±390	0.35±0.13	–
Mrk 1271	11±7	–	–	11±7	77±22	0.14±0.05	–
NGC 450	322±215	–	129±51	451±221	2044±147	0.22±0.08	0.40±0.14
NGC 4385	3037±1534	1208±960	972±634	5217±2288	25740±7610	0.20±0.07	0.72±0.25
NGC 4861	522±288	65±3	58±35	586±290	4375±489	0.15±0.05	0.24±0.08
NGC 5430	4761±2520	–	999±435	5761±2558	66149±17776	0.09±0.03	0.21±0.08
NGC 5471	2±1	–	–	2±1	44±2	0.05±0.02	–
NGC 6764	2812±1687	859±42	1750±906	5421±2231	79325±14771	0.07±0.02	0.93±0.33
NGC 6764	2380±1457	735±49	1606±817	4721±1943	56180±11250	0.08±0.03	0.98±0.35
NGC 7714A	1920±1288	869±18	1596±883	5295±2277	44282±2655	0.12±0.04	0.87±0.31
NGC 7714B	451±255	–	–	451±255	3276±357	0.14±0.04	–
UM 48	1654±1279	–	353±234	2007±1300	38967±6385	0.05±0.02	0.21±0.08

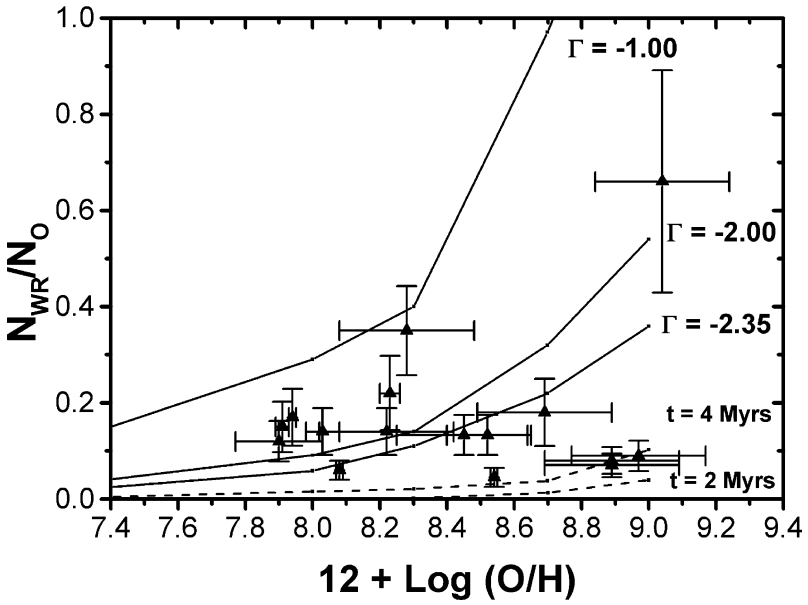

Figure 8. $N_{\rm WR}/N_{\rm O}$ versus 12 + log(O/H) for the galaxies in our sample. Predictions of Schaerer & Vacca (1998) models for instantaneous bursts (solid line) and of Starburst 99 (Leitherer et al. 1999) for extended bursts of star formation of 2 and 4 Myr (dashed line) are overplotted. The lines are labelled with the IMF slopes.

indicating the presence of red giants and supergiants (Bica & Alloin 1986). The presence of late-type stars further supports the idea of an extended burst with an age <7 Myr. In Fig. 10 we present the spectra of these four high-metallicity galaxies which show apparent TiO bands (∼λ6250) and a blend of Fe I + Ba II + Ca Iλ6495, which are spectral features of characteristic of late-type stars.

Alternatively, Pindao et al. (2002) suggest that corrections to the evolutionary models can reproduce the low observed $N_{\rm WR}/N_{\rm O}$ ratios using an instantaneous burst. They invoke the uncertainties in synthesis models of WR bumps to explain their results, because the WR line luminosities show a large scatter in the WNL calibration sample of SV98 with Galactic and Large Magellanic Cloud objects. A dependence between the WR luminosity and the bolometric stellar luminosity may cause this discrepancy. The WR line luminosity L_{4686} is observed to increase with increasing bolometric stellar luminosity. They suggest a more precise analysis, splitting the bolometric stellar luminosity in two domains: $\log(L/\,{\rm L}_{\odot}) < 6$ and $\log(L/\,{\rm L}_{\odot}) > 6$. The different average line luminosities for each domain are $L_{4686} = 5.6 \times 10^{35}$ erg s^{-1} for $\log(L) < 6$ and $L_{4686} = 3.1 \times 10^{36}$ erg s^{-1} for $\log(L) > 6$. Using these values in synthesis models leads to a reduction in the predicted number of WNL stars. Note that the line luminosity for a WNL star with $L > 6\,{\rm L}_{\odot}$ is almost twice as large as that adopted by SV98 for their Galactic calibration sample. Using these values in the synthesis models, their observed WR features can be reproduced with an instantaneous burst and a standard Salpeter IMF (Pindao et al. 2002). The recalibrated (lower) luminosity of WN stars used in models leads to a significant reduction in the WR bump intensity in the bursts with ages ⩾4–5 Myr.

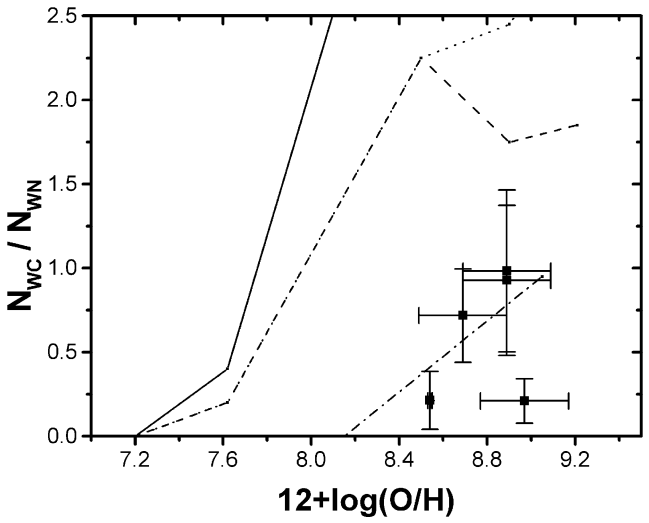

Figure 9. $N_{\rm WC}/N_{\rm WN}$ versus $12 + \log({\rm O/H})$ for the high-metallicity galaxies in our sample. Predictions of Schaerer & Vacca (1998) models for maximum value for instantaneous bursts (solid line) and SGIT00 extended bursts of 2–4 Myr (dashed lines) are overplotted. The dot-dashed line (bottom right) shows the observed trend of WC/WN with metallicity in Local Group galaxies derived empirically from observations by Massey & Johnson (1998).

Only the youngest bursts with very high EW(Hβ) are dominated by very luminous WNL stars. For objects with low $N_{\rm WR}/N_{\rm O}$ ratios, if we apply the suggested correction to the L_{4686} luminosities in the actual observations (instead of the models), and recalculate the number of WN stars at the highest metallicities (dominated by low-luminosity WNL stars), the lower luminosity of WNL stars can increase the fraction of WN stars by a factor of ∼2–2.3 (GIT00). With this change in assumed luminosity, we are unable to reproduce the standard instantaneous burst model predictions for the $N_{\rm WR}/N_{\rm O}$ ratio in the highest-metallicity galaxies. This analysis confirms that the low values of $N_{\rm WR}/N_{\rm O}$ for objects with $12 + \log({\rm O/H}) > 8.4$, obtained for NGC 4385, 5430, 6764 and UM 48, require an extended burst with a Salpeter IMF slope.

6 CONCLUSION

In this paper, we have presented a spectroscopic study of 14 WR galaxies from the sample of SCP98, as well as NGC 450 for which the WR features are newly detected. Our goals were to search for and confirm the presence of WN and WC stars, and to compare the results with predictions from evolutionary synthesis models (SV98). We have tested the agreement of these models with observations for a large range of metallicities, spanning $7.90 \leqslant 12 + \log({\rm O/H}) \leqslant 9.04$.

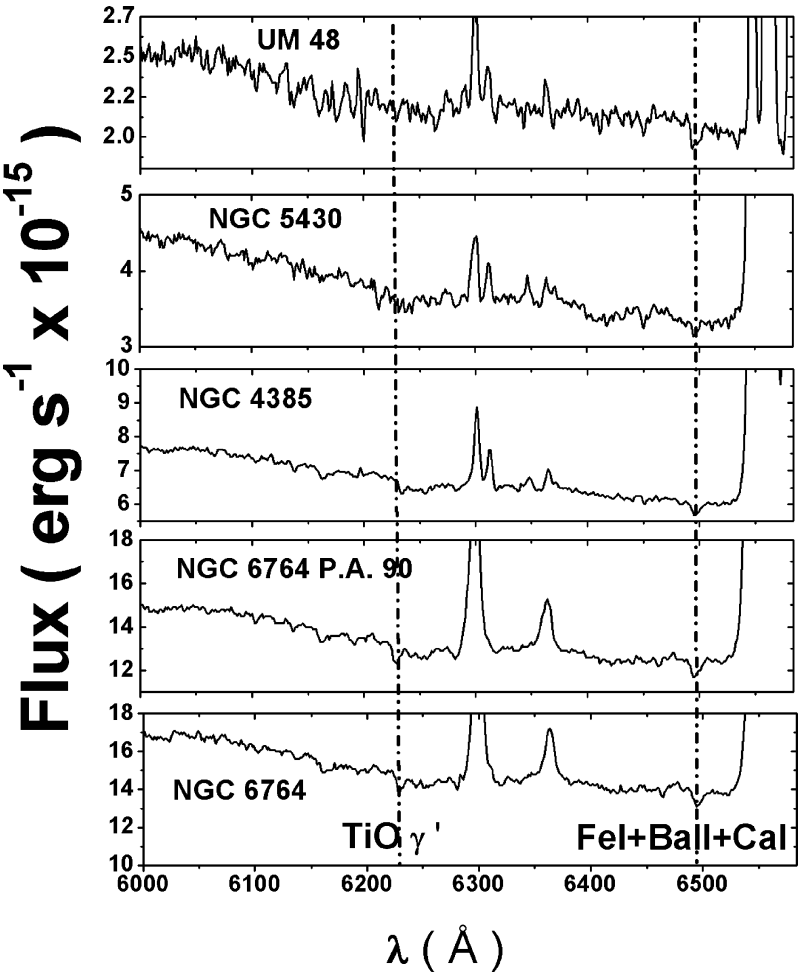

Figure 10. Spectral region showing TiO bands (∼λ6250) and narrow Fe I + Ba II + Ca I λ6495 for the high-metallicity galaxies NGC 4385, 5430, 6764 (PAs 67° and 90°), 5471 and UM 48.

Our main results can be summarized as follows.

(i) The broad WR emission in the blue region of the spectrum, the blend of N IIIλ4640, C IIIλ4650, C IVλ4658 and He IIλ4686 emission lines, is present in all 14 galaxies. The WR population in these galaxies is dominated by late WN stars. However, the red bump produced by the emission of broad C IVλ5808 from early WC stars is detected in only nine galaxies.

(ii) The weak, broad WR emission line C IIIλ5696 is detected in six galaxies, which suggests the presence of late WCL stars in these objects. This line is expected in high-metallicity environments (GIT2000). A good example of this is Mrk 309, with a metallicity of $12 + \log(\mathrm{O/H}) = 9.04$, where this line is strong.

(iii) We found good agreement when comparing the relative numbers of WR and O stars ($N_{\mathrm{WR}}/N_{\mathrm{O}}$) obtained from observations and those predicted by the evolutionary synthesis models of SV98 for low-metallicity galaxies. The ratio $N_{\mathrm{WR}}/N_{\mathrm{O}}$ in these galaxies can be explained by a burst of star formation. The $N_{\mathrm{WR}}/N_{\mathrm{O}}$ value and the observed equivalent widths of the blue and red bumps also compare favourably with SV98 predictions. We found that it is necessary to invoke an IMF slope between $-2 \lesssim \Gamma \lesssim -2.35$ and an instantaneous star formation event to explain the observed $N_{\mathrm{WR}}/N_{\mathrm{O}}$ ratios in low-metallicity regimes.

(iv) For NGC 4385, 5430, 6764 and UM 48, the $N_{\mathrm{WR}}/N_{\mathrm{O}}$ ratios are lower than the predictions of models with an instantaneous burst for metallicities of $12 + \log(\mathrm{O/H}) > 8.4$. The existence of an extended burst is supported by the presence of TiO bands ($\sim\lambda$6250) in these objects spectra. The presence of this older stellar population is indicative of the necessary time elapsed since the burst for stars to evolve through this phase. The $N_{\mathrm{WN}}/N_{\mathrm{WC}}$ ratios combined with their high metallicity suggest these objects are in the late stages of their WR episodes ($\geqslant$5.3 Myr), when WN stars are present while the number of WC stars drops to zero (SV98). The observations can be better represented using extended starbursts with durations of 2–4 Myr and Salpeter IMF slope.

(v) Massive stellar evolution models predict that the relative number of WR stars increases when metallicity increases (Maeder & Meynet 1994; SV98). Our results do not confirm this trend. The partial disagreement between our results and the models may arise from large uncertainties in the luminosity of a single WR star and the uncertainties associated with the best choice of the dominant contribution of WR star subtype in the high-metallicity regime.

The massive stellar populations in WR galaxies can be better understood if studies like this one are combined with other stellar population investigations. A detailed spectral study in the infrared of molecular bands and low-ionization absorption lines can provide information about older stellar populations in a starburst (Origlia et al. 1999; GIT00). Spectroscopy in the ultraviolet (912–1800 Å) can provide information about the young star population in galaxies. This ultraviolet spectral range contains resonant spectral lines of O VIλ1035, Si Vλ1400 and/or C IVλ1550 that are spectral signatures of young massive stars (Leitherer et al. 2002). The combination of the infrared and ultraviolet yields information on the current stellar populations, and constrains the upper and lower limits of time elapsed since the burst (Oliva et al. 1999; Leitherer et al. 2002). Additionally, analysis of the α-element abundances can provide additional constraints on the age of the burst and consequently the number of massive stars (Lanfranchi & Friaça 2003).

ACKNOWLEDGMENTS

It is a pleasure to thank Sueli M. M. Viegas for discussions and contributions with helpful comments. IFF is grateful to the staff of the Laboratoire d'Astrophysique, Observatoire Midi-Pyrénées for their kind hospitality. This international collaboration was possible thanks to the financial support of IAG-USP, FAPESP grant No 99/12721-5 and of L.A.O.M.P. URA 285.

REFERENCES

Allen S. W., 1995, MNRAS, 276, 947
Allen D. A., Wright A. E., Goss W. M., 1976, MNRAS, 177, 91
Barth C. S., Cepa J., Vilchez J. M., Dottori H. A., 1994, AJ, 108, 2069
Bica E., Alloin D., 1986, A&A, 162, 21
Brocklehurst M., 1971, MNRAS, 153, 471
Calzetti D., 1997, AJ, 113, 162
Cardelli J. A., Clayton G. C., Mathis J. S., 1989, ApJ, 345, 245 (CCM89)
Castañeda H. O., Vilchez J. M., Copetti M. V. F., 1990, ApJ, 365, 164
Conti P. S., 1991, ApJ, 377, 115
Contini T., Davoust E., Considere S., 1995, A&A, 303, 440
Contini T., Wozniak H., Considere S., Davoust E., 1997, A&A, 324, 41
Contini T., Kunth D., Mas-Hesse M., Arribas A., 2001, in Rocca-Volmerang B., Sol H., eds, EAS Pub. Series, Vol. 1, Active Galactic Nuclei in Their Cosmic Environment. EDP Sciences, Les Ulis, France, p. 163
Contini T., Treyer M. A., Sullivan M., Ellis R. S., 2002, MNRAS, 330, 75
Dinerstein H. L., Shields G. A., 1986, ApJ, 311, 45
Durret F., 1990, A&A, 229, 351
Durret F., Tarrab I., 1988, A&A, 205, 9
Eckart A., Cameron M., Boller T., Krabbe A., Blietz M., Nakai N., 1996, ApJ, 472, 588
Edmunds M. G., Pagel B. E. J., 1984, MNRAS, 211, 507
Evans I. N., 1986, ApJ, 309, 544
Gil de Paz A., Aragon-Salamanca A., Gallego J., Alonso-Herrero A., 2000, MNRAS, 316, 357
González-Delgado R. M., Perez E., Diaz A. I., Garcia-Vargas M. L., Terlevich E., Vilchez J. M., 1995, ApJ, 439, 604
Grevesse N., Anders E., 1989, AIPC, 183, 1
Grevesse N., Sauval A. J., 1998, Space Sci. Rev., 85, 161
Guseva N. G., Izotov Y. I., Thuan T. X., 2000, ApJ, 531, 776 (GIT00)
Heckman T. M., González R. M., Leitherer C., Meurer G. R., Krolik J., Wilson A. S., Koratkar A., Kinney A., 1997, ApJ, 482, 114
Ho L. C., Filippenko A. V., Sargent W. L., 1995, ApJS, 98, 477
Izotov Y. I., Thuan T. X., 1998, ApJ, 500, 188
Izotov Y. I., Thuan T. X., Lipovetsky V. A., 1994, ApJ, 435, 647
Izotov Y. I., Thuan T. X., Lipovetsky V. A., 1997, ApJS, 108, 1
Kell W. C., 1982, PASP, 94, 765
Kell W. C., 1987, A&A, 172, 43
Kewley L. J., Heisler C. A., Dopita M. A., Lumsden S., 2001, ApJS, 132, 37
Kobulnicky H. A., Kennicutt R. C. Jr., Pizagno J. L., 1999, ApJ, 514, 544
Kovo O., Contini T., 1999, IAUS, 193, 604
Kunth D., Joubert M., 1985, A&A, 142, 411
Lanfranchi G. A., Friaça A. C. S., 2003, MNRAS, 343, 481
Leitherer C. et al., 1999, ApJS, 123, 3
Leitherer C., Li I.-H., Calzetti D., Heckman T. M., 2002, ApJS, 140, 303
McCall L. M., 1984, MNRAS, 208, 253
McCall L. M., Rybski P. M., Shields G. A., 1985, ApJS, 57, 1 (MRS85)
McGaugh S. S., 1991, ApJ, 380, 140
Maeder A., 1991, A&A, 242, 93
Maeder A., Conti P. S., 1994, ARA&A, 295, 171
Maeder A., Meynet G., 1994, A&A, 287, 816
Masegosa J., Moles M., del Olmo A., 1991, A&A, 244, 273
Mas-Hesse J. M., Kunth D., 1991, A&AS, 88, 399
Massey P., Johnson O., 1988, ApJ, 505, 793
Mattila S., Meikle W. P. S., 2001, MNRAS, 324, 325
Meynet G., 1995, A&A, 298, 767
Oke J. B., Gunn J. E., 1982, PASP, 94, 586

Oliva E., Origlia L., Maiolino R., Moorwood A. F. M., 1999, A&A, 350, 9
Origlia L., Goldader J. D., Leitherer C., Schaerer D., Oliva E., 1999, ApJ, 514, 96
Osterbrock D. E., Cohen R. D., 1982, ApJ, 261, 64 (OC82)
Peimbert M., Costero R., 1969, Bol. Obs. Tonantz. Tacub., 5, 3
Peimbert M., Sarmiento A., Fierro J., 1991, PASP, 103, 815
Pettini M., Pagel B. E. J., 2004, MNRAS, 348, 59
Pilyugin L. S., 2000, A&A, 362, 325
Pilyugin L. S., 2001a, A&A, 369, 594
Pilyugin L. S., 2001b, A&A, 374, 412
Pindao M., Schaerer D., González-Delgado R. M., Stasińska G., 2002, A&A, 394, 443
Rosa M. R., Benvenuti P., 1994, A&A, 291, 1
Salzer J., 1989, ApJ, 347, 152
Salzer J. J., MacAlpine G. M., Boroson T. A., 1989, AJ, 70, 477
Schaerer D., Vacca W. D., 1998, ApJ, 497, 618 (SV98)
Schaerer D., Contini T., Pindao M., 1999a, A&AS, 136, 35 (SCP99)
Schaerer D., Contini T., Kunth D., 1999b, A&A, 341, 399
Schaerer D., Guseva N. G., Izotov Y. I., Thuan T. X., 2000, A&A, 362, 53 (SGIT00)
Schmitt H., Storchi-Bergmann T., Cid Fernandes R., 1998, AAS, 193, 608
Steigman G., Viegas S. M., Gruenwald R., 1997, ApJ, 490, 187
Sugai H., Taniguchi Y., 1992, AJ, 103, 1470
Vacca W. D., 1994, ApJ, 421, 140
Vacca W. D., Conti P. S., 1992, ApJ, 401, 543 (VC92)
van Breugel W., Filippenko A. V., Heckman T., Miley G., 1985, ApJ, 293, 83
Veilleux S., Osterbrock D. E., 1987, ApJS, 63, 295
Vogel S., Engels D., Hagen H.-J., Groote D., Wisotzki L., Cordis L., 1993, A&AS, 98, 193
Weedman D. W., Feldman F. R., Balzano V. A., Ramsey L. W., Sramek R. A., Wuu C.-C., 1981, ApJ, 248, 105

APPENDIX A: REMARKS ON INDIVIDUAL OBJECTS

In this section we present a brief description of some specific properties of each galaxy in our sample. By doing so we can address specific issues related to these objects, compare with results from other authors, and obtain important information for the analysis of the population as a whole.

Fairall 44. Kovo & Contini (1999) reported on the blue bump in their systematic search for WR stars in young starburst galaxies. We report on the presence of WN stars in this galaxy. We find that the WR/O ratio is 0.24.

III Zw 107. Kunth & Joubert (1985) reported on a moderately strong emission band at 4686 Å due to WR stars in III Zw 107 S. We report on the presence of N IIIλ4640 and He IIλ4886 broad emission lines in this galaxy. The WR/O ratio is 0.12.

Mrk 309. This bright ultraviolet continuum galaxy has broad emission features at N IIIλ4640 and He IIλ4686 from WR stars noted by OC82. They found that the number of WR stars is comparable to the number of O stars in this galaxy and the nuclear region of NGC 6764. We note the presence of N IIIλ4640 and He IIλ4686 in the blue bump and C IIIλ5696 in the red bump in our spectrum of this galaxy. We find that the number of WR stars is similar to that of O-type stars in the nuclear region of Mrk 309. Our results are in good agreement with SGIT00.

Mrk 475. Broad He IIλ4686 and N IIIλ4640 emission lines were first noted by Conti (1991). Strong blue and red bumps were detected by ITL94. GIT00 identified features of Si IIIλ4565, He IIλ4686, HeI,N IIλ5047 and C IVλ5808, where the blue bump is strongly contaminated by nebular emission. We confirm the results of GIT00, and find a WR/O ratio of 0.17.

Mrk 712. Contini et al. (1995) reported on the discovery of emission from WR stars in the giant H II region 4.5 arcsec south of the nucleus. They estimated a WN/O ratio of 0.2 from the He IIλ4686 luminosity. The [Ar V] emission line in their spectrum showed that the H II region is strongly ionized by hot WR stars. The WN/WO ratio indicated a very young starburst episode and a flat IMF with slope Γ between -1 and -2. We use the SV98 evolution models to compare with our observational results (Section 6.2).

Mrk 1271. Izotov & Thuan (1998) detected a broad blue bump. GIT00 identified the N IIIλ4512, Si IIIλ4565, N IIλ4620 and He IIλ4686 emission lines, and possibly C IVλ5808 in their high-quality spectrum. They reported the blue bump as being strongly contaminated by nebular emission. We confirm only the presence of the He IIλ4686 broad line in the nuclear region of this galaxy. The C IVλ5808 broad line is not detected in our spectrum of Mrk 1271. The WR/O ratio is 0.14.

NGC 450. There is no mention of WR detection in this galaxy in the literature. We report on a ratio of WR/O = 0.22. The models of SV98 for an instantaneous star formation episode predict a flat IMF slope ($\Gamma = -1$ to -2) to explain the presence of WR stars in this low-metallicity galaxy.

NGC 4385. He IIλ4686 and N IIIλ4640 WR features are present in this starburst galaxy, according to Durret & Tarrab (1988). An optical spectrum by Salzer (1989) shows essentially the same features. Conti (1991) has identified a narrow emission feature near 4660 Å as [Fe III], while Salzer et al. (1989) identifies it as C IV. We detect N IIIλ4640 and He IIλ4686 in the blue bump and C IIIλ5696 and C IVλ5808 in the red bump. We find a high number of WR stars compared to O stars. The WR/O ratio is 0.13 for the nuclear region of NGC 4385.

NGC 4861. Dinerstein & Shields (1986) and Izotov, Thuan & Lipovetsky (1997) detected the blue and red bumps. GIT00 identified N IIIλ4512, Si IIIλ4565, N Vλ4619, He IIλ4686 and C IVλ5808 broad emission lines, and a blue bump strongly contaminated by nebular emission. Even with their high-quality spectrum, the N IIIλ4640 and C IVλ4658 lines appear blended. In our spectrum of the central region of this galaxy, we can resolve the lines of the blue bump. We report on the presence of C IIIλ5696 and C IVλ5808 broad emission lines due to WC stars.

NGC 5430. A strong emission feature near 4650 Å due to WR stars in the spectrum of a bright region south-east of the galactic centre was noted by Kell (1982). He identified N IIIλ4640 and He IIλ4686 emission lines as coming from WN stars (Kell 1987). No strong emission features are seen in the *International Ultraviolet Explorer* (*IUE*) spectrum of this source. A relatively older stellar population appears in the centre of NGC 5430. According to Kell (1987), the knot 20 arcsec south-east of the nucleus might be a separate galaxy interacting with NGC 5430. For this knot we measure the N IIIλ4640 and He IIλ4686 blue bump broad components, as well as the C IIIλ5696 and C IVλ5808 broad emission lines. A high WR/O ratio of 0.09 is found for NGC 5430.

NGC 5471. This is a massive giant H II region located in M101. Mas-Hesse & Kunth (1991) found WR–He IIλ4686/ Hβ = 0.02 and a 3.5-Myr burst. NGC 5471 seems to be dominated by a well-defined burst of star formation. A broad He II emission line (FWHM $\simeq$ 2000 km s^{-1}) was detected in this region by Castañeda, Vilchez & Copetti (1990) and was confirmed by Mas-Hesse & Kunth (1991). We find a low ratio WR/O = 0.04 for this galaxy.NGC 6764. OC82 noted the presence of broad N IIIλ4640 and He IIλ4686 emission line features from WR stars. They attributed the 4660-Å emission

line to C III and not to [Fe III] forbidden emission. The similarity of the overall emission-line spectrum of NGC 6764 to that of dwarf galaxies and to certain giant H II regions attracted the attention of these authors. We observed this object at two PAs, 90° and 46°. We find WN and WC stars in the nuclear region of this galaxy. For both PAs the number of WR stars is comparable to that of O-type stars.

NGC 7714. Weedman et al. (1981) called this object a 'prototype starburst' galaxy. van Breugel et al. (1985) noted the spectral similarity of NGC 7714 to Minkowski's object and extragalactic H II regions. They reported this galaxy as having weak WR emission features near He IIλ4686. Conti (1991) called attention to the importance of NGC 7714 for understanding the relation between starbursts and the presence of WR stars in this type of galaxy. We found WR stars in two regions of NGC 7714. In the nuclear region we find WR/O = 0.08, while in the secondary H II region, WR/O = 0.14. In the nuclear regions we were able to measure the C IIIλ5696 and C IVλ5808 broad emission lines due to WC stars.

UM 48. A systematic search for WR features in this galaxy was carried out by Masegosa et al. (1991). The authors reported on the presence of a WR blue bump. They assumed that the global WR detection rate depends on the metallicity and they analysed the SN IIe contribution to the blue bump. They concluded that a large blue bump luminosity should be expected in regions with SN contamination. We did not detect the N IIIλ4640 broad emission line in this galaxy. We measure the WC broad emission line C IVλ5808.

This paper has been typeset from a TEX/LATEX file prepared by the author.